The Meteoritical Society

Meteoritics & Planetary Science 46, Nr 1, 53–78 (2011)
doi: 10.1111/j.1945-5100.2010.01138.x

Ejecta–megaregolith accumulation on planetesimals and large asteroids

Paul H. WARREN*

Institute of Geophysics, UCLA, Los Angeles, California 90095–1567, USA
*Corresponding author. E-mail: pwarren@ucla.edu

(*Received 27 January 2010; revision accepted 25 September 2010*)

Abstract–Megaregolith accumulation can have important thermal consequences for bodies that lose heat by conduction, as vacuous porosity of the kind observed in the lunar megaregolith lowers thermal conductivity by a factor of 10. I have modeled global average ejecta accumulation as a function of the largest impact size, with no explicit modeling of time. In conjunction with an assumed cratering size-distribution exponent b, the largest crater constrains the sizes of all other craters that significantly contribute to a megaregolith. The largest impactor mass ratio is a major fraction of the catastrophic-disruption mass ratio, and in general the largest crater's diameter is close to the target's diameter. Total accumulation is roughly 1–5% of (and proportional to) the target's radius. Global accumulations estimated by this approach are higher than in the classic Housen et al. (1979) study by a factor of roughly 10. This revision is caused mainly by higher (typical) largest crater size. For $b \sim 2$, the single largest crater typically contributes close to 50% of the total of new (nonrecycled) ejecta. Megaregolith can be destroyed by sintering, a process whose pressure sensitivity makes it effective at lower temperature on larger bodies. Planetesimals ~100 km in diameter may be surprisingly well suited (about as well suited as bodies two to three times larger in diameter) for attaining temperatures conducive to widespread melting. A water-rich composition may be a significant disadvantage in terms of planetesimal heating, as the shallow interior may be densified by aqueous metamorphism, and will have a low sintering temperature.

INTRODUCTION

The larger planetesimals, asteroids, and rocky natural satellites are/were invariably blanketed by an accumulation of impact-crater ejecta (megaregolith). The extent of that accumulation is of interest for various reasons. The early bodies underwent rapid thermal evolutions that determined the course of their metamorphic/igneous modification, and ultimately influenced the origin and evolution of the planets. The thermal evolution was determined by a competition: heat generation, probably mainly by ^{26}Al ($t_{1/2}$ = 0.72 Ma), versus heat loss, which in small bodies occurs mainly by conduction. Megaregolith–ejecta accumulation can have important thermal consequences for such a body. The rate of loss is a function of the thermal conductivity k of the outer layers. Vacuous porosity of the kind observed in the lunar megaregolith lowers conductivity by a factor of approximately 10 (Warren and Rasmussen 1987). Recent thermal models make a range of extreme and, in terms of evolutionary implications, divergent assumptions about k. At one extreme are models (e.g., Ghosh and McSween 1998; Merk et al. 2002; Wilson et al. 2008) that simply assume a solid rock like k. At another extreme, some (Hevey and Sanders 2006; Sahijpal et al. 2007) assume that k is similar to that of lunar surface fines (i.e., lower by a factor of approximately 2000 compared to the solid-rock k: Langseth et al. 1976) prevails until, with rising T, sintering suddenly transforms the material to rock-like k. The megaregolith, for the purposes of this work, is defined as the body's layer of accumulated impact-crater ejecta, exclusive of material that may have become extensively modified (sintered) to a low porosity. This article is concerned with megaregolith development on bodies of diameter d_B between approximately 100 km and Moon-sized (3476 km); i.e., mass between 10^{18} and

10^{23} kg. Megaregolith is also important as the outer shell of porous, weak material into/through which later impacts transpire; as the usual context for spall-off of chunks that may become meteorites; and as the context for remote sensing observations.

The blast-out and accumulation cycle that produces megaregolith leads to an increase in porosity, by a factor estimated (e.g., Melosh 1989; Richardson 2009) to be approximately 20%. In the context of an atmosphereless planetesimal, this porosity probably tends to be vacuous, like the porosity of the Moon's regolith and megaregolith. Vacuous porosity leads to a marked diminution of thermal conductivity k (Wechsler et al. 1972; Horai and Winkler 1980). Yomogida and Matsui (1984) found analogous effects with mildly porous chondritic materials. Models that assume gas pressure is not $<<0.1$ MPa within the pores (e.g., a model used in planetesimal modeling by Ciesla et al. 2009) vastly overestimate the k of vacuous–porous materials. The lunar data (summarized in Fig. 1) show that vacuous porosity yields a reduction in k along a single exponential relationship, whether the material is a cohesive breccia or a loose soil. Even the igneous (nonfracture) porosity in unbrecciated mare basalt appears to have almost the same effect (regarding sample 70017, see the caption of Fig. 1).

A low-k planetary layer may be analogized to a resistor in an electrical circuit. The thermal resistance of each layer is proportional to $(1/k_{i\text{-}o})(1/r_i - 1/r_o)$, where r_o and r_i are the fractional radii of the outer and inner boundaries of the layer (e.g., Sucec 1975). The resistances are additive. As a crude illustration of the potential importance of the insulating layer, the steady-state, internal heat generation neglected, heat flow q out of the body shown in Fig. 2 would be

$$q = \frac{4\pi(T_1 - T_3)}{(1/k_{1-2})(1/r_1 - 1/r_2) + (1/k_{2-3})(1/r_2 - 1/r_3)}. \quad (1)$$

Results from Equation 1 for the relative q implied by various assumptions regarding the megaregolith's thickness and conductivity are shown in Fig. 2. For example, suppose a body of order 100–1000 km in diameter d_B has a 2 km megaregolith, with $k = 0.1\times$ solid rock, atop a 6 km conductive solid-rock layer, below which the body is approximately isothermal due to the rapidity of primordial heating in relation to thermal diffusivity. A planetesimal that undergoes rapid, uniform heating will develop an approximately isothermal deep interior (inward of r_1 in Fig. 2), as the influence of radiative heat loss from the surface penetrates only to a "skin" depth that according to

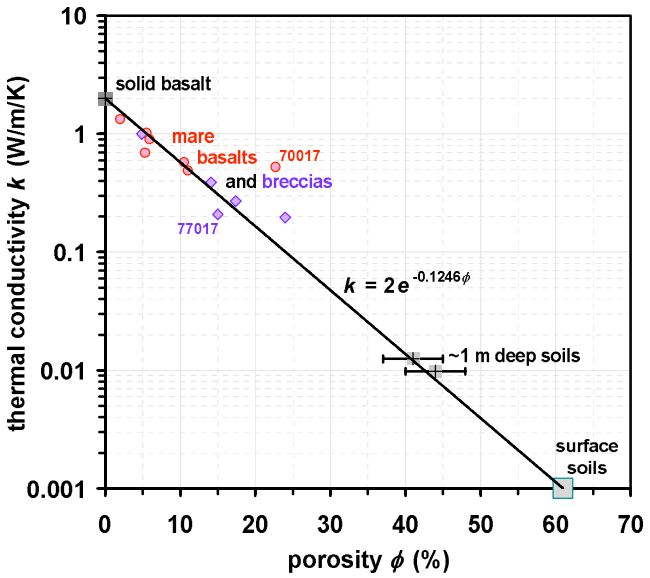

Fig. 1. Thermal conductivity (k) at 300 K, plotted as a function of vacuous porosity for lunar rocks and soils. Data are from Horai and Winkler (1980) and other sources cited in Warren and Rasmussen (1987), most notably, for the 1 m deep soils, k from Langseth et al. (1976; their fig. 6) and porosity from Carrier et al. (1991). The breccias are mostly impact melt breccias, except for 77017 (porosity = 15%) which is a fragmental breccia, and 10065 (porosity 24%), which is a regolith breccia. The exponential equation for the line between solid rock and (average) surface soil is $k = 2e^{-0.1246\varphi}$. The one clear deviant from the trend, mare basalt 70017, is unusually coarse-grained, and Horai and Winkler (1976) used an uncommonly small sample for their 70017 measurements.

Wilson et al. (2008) is approximately 8 km (as will be discussed below, the skin depth is a function of time, k, and heat production, but 8 km is a plausible result for a small body heated by ^{26}Al for several Ma). Figure 2 indicates that a 2 km megaregolith layer, with $k = 0.1\times$ the deep (solid) interior k, will reduce heat loss from the deeper interior by a factor of 3 in comparison to the rate with the higher k throughout. The same approximate total resistance would result if just 0.02 km of powdery regolith with $k = 0.001 \times$ solid rock were separated from the near-isothermal core by a 7.98 km solid-rock layer.

For the best known megaregolith-covered body, the Moon, based on an earlier version of Fig. 1, coupled with a compilation of porosities in lunar breccias (average: 17 ± 10%), Warren and Rasmussen (1987) estimated that the k_{MR} of the megaregolith is approximately 0.1 times that of solid rock. In general, porosity is expected to be higher on smaller bodies, with their lower gravity and internal pressure, and lower potential for igneous activity and sintering after the main, late-accretionary era of impact cratering. The

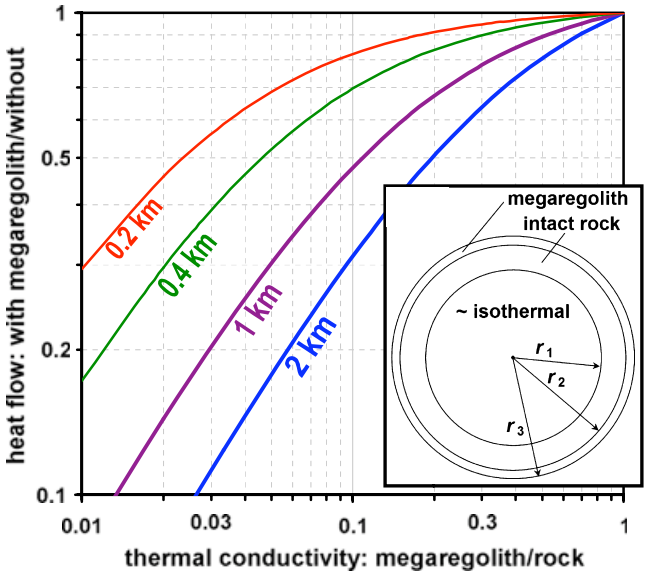

Fig. 2. Results from application of Equation 1 to cooling of a megaregolith-covered body (shown in schematic cross section in the inset): relative steady-state heat flow q as a function of the relative conductivity k_{MR} of the megaregolith, shown for a range of assumed megaregolith thickness. The models shown assume the depth to the approximately isothermal deep interior (depth to r_1) is 8 km (Wilson et al. 2008; see text) and that the body is approximately 500 km in diameter d_B. (Results are not very sensitive to d_B; e.g., for megaregolith thickness of 1 km and $k_{MR}/k_{rock} = 0.1$, relative q varies by only a factor of 1.074 as d_B ranges from 100 to 1000 km.) The actual situation is never as simple as modeled here, as the body is being heated from within by, e.g., (in the case of an early planetesimal) ^{26}Al.

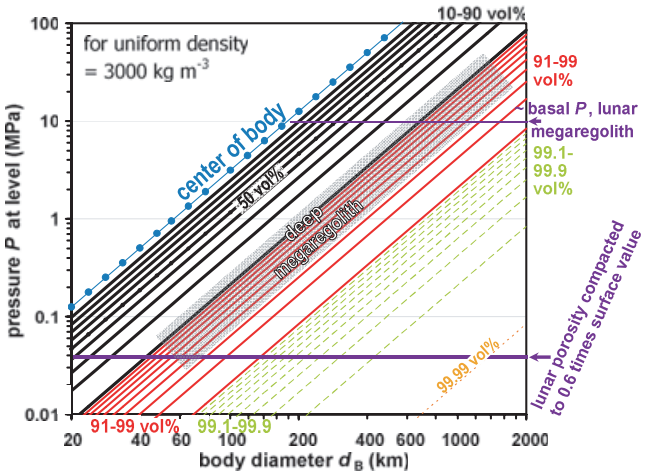

Fig. 3. Pressures within bodies of uniform 3000 kg m^{-3} density, calculated using equation 2–64 of Turcotte and Schubert (1982). To scale to a different density, multiply the indicated P times (density/3000) squared. Grey region indicates estimated range of P for deepest, most sinter-densification prone portion of megaregolith as modeled (assuming $b = 2$ and $D_L/d_B = 0.6$–1) in this work.

near-surface hydrostatic pressure–depth gradient dP/dz is directly proportional to d_B, and the P at any given r/r_B scales as d_B^2 (Fig. 3; density variations may alter this nominal P-distribution, but only to a mild extent). On a small (say $d_B < 100$ km) body, the average megaregolith porosity could conceivably be as high as 40%, implying a reduction in k by a factor of 10^2 relative to the solid-rock k (Fig. 1).

Housen et al. (1979) authored the classic study of the development of asteroidal ejecta accumulations (cf. Housen and Wilkening 1982). However, their approach focused on the issue of crater saturation for a "typical" surface region "exterior to sparsely scattered, large anomalous craters"; and on that region's evolution, and in particular its elevation evolution, as a function of time (cf. Ward 2002). An approach focused on time and saturation can be useful for application to powdery regolith (sensu stricto) on asteroids, especially asteroids that may have acquired fresh-rocky surfaces at some relatively recent date. But for the more basic purpose of constraining global impact ejecta accumulation thickness, timing is an ancillary issue, and introduces unnecessary complication. It is precisely the few "large anomalous" craters that preponderate in contributions to a global megaregolith. Moreover, in some important respects, such as depth and volume of the excavation/ejection zone, the Housen et al. (1979) model has been superseded by modern cratering physics interpretation. My model builds from the simple premise that impactors, and the craters they produce, conform (approximately) to a power-law size–frequency distribution; which implies that an estimate for the magnitude of the single largest crater implicitly constrains the sizes of all other craters large enough to be significant contributors to the final megaregolith. The key issue of the (typical or average) size of the largest crater is admittedly difficult to constrain. For now, suffice to note that 4 Vesta's largest crater is a 460 km basin whose transient crater probably had a diameter of approximately 310 km, or 0.58 times the diameter of Vesta itself (Asphaug 1997; Thomas et al. 1997).

MEGAREGOLITH ACCUMULATION MODEL

Volume and Depth Provenance of Ejecta from an Individual Crater

Craters are complex and diverse. The approach of using any single equation to characterize the relationship between crater size (D_t) and the globally averaged thickness z_1 of the crater's ejecta is justifiable, however, because our real aim is to evaluate the aggregate ejecta thickness z_A from a multitude of craters

on a multitude of bodies. Housen et al. (1979) modeled the excavation/ejection zone of a nascent impact crater as a spherical cap with depth/diameter ratio of 0.2. As discussed by, e.g., Melosh (1989), π-group scaling and observational constraints imply that the ejection/excavation zone may be better modeled as parabolic and with depth/diameter ratio approximately 1/10 to 1/8. Haskin et al. (2003) thus modeled the volume of ejecta from a crater as

$$V_1 = 0.09\pi R_t^3, \tag{1a}$$

where R_t is the radius of the ejection zone, which coincides with the radius of the transient crater. The factor of 0.09 (rather than the depth/diameter ratio of 0.10) is meant to compensate for a zone near the center-bottom of the transient crater that is pushed down (or vaporized) but not ejected (cf. Melosh's fig. 5.13; or figs. 2 and 3 of Wada et al. 2004). Compared with the spherical cap (and 2× deeper) model of Housen et al. (1979), the V_1 implied by Equation 1a is 0.43 times less (or even smaller, considering that Equation 1a uses the transient crater radius, whereas Housen et al. 1979, drew little distinction between transient and final crater radius).

Maxwell's (1977) analytical model of excavation flow suggests that the ejection zone is deeper toward its rim than in the paraboloid model. This model assumes that flow velocity decreases as an inverse power of radial distance r^{-Z} from the explosive center. The Z-model is not perfect; a precise fit to the excavation flow probably requires assuming that Z is not a constant but a variable function of time (Anderson et al. 2003; cf. Yamamoto et al. 2009). Still, Maxwell's (1977) model assuming $Z \sim 3$ gives a good fit to the excavation flow and the shape of the ejection volume, as constrained by a variety of observations (Melosh 1989; Wada et al. 2004). Croft (1980) showed that the volume of the ejection zone in this model is

$$V_1 = \left(\frac{2}{3}\right)\pi R_t^2\left(1 - \frac{3}{(Z+1)}\right). \tag{1b}$$

A depth/diameter ratio of 0.10, matching Equation 1a, requires $Z = 2.734$. The factor $(1–(3/Z + 1))$ then becomes 0.197, and with R_t set at unity Equation 1b implies an ejection volume 1.45 times greater than Equation 1a. A model for π-group scaling developed by Holsapple (2003; cf. Housen et al. 1983; and Holsapple 1993) similarly implies a factor of 1.33 greater volume of excavation than Equation 1a. In the absence of strong evidence for choosing among the Equation 1a, Equation 1b, and Holsapple models, for purposes of further discussion the volume of the ejection zone will be modeled as:

$$V_1 = 0.11\pi R_t^3. \tag{1c}$$

The contribution z_1 of this volume of ejecta to the average global thickness of megaregolith z_A in a spheroidal body may be approximated by dividing V_1 by the surface area, $4\pi {r_B}^2$, where r_B is the radius of the body, which yields

$$z_1 = 0.0275\left(\frac{R_t^3}{r_B^2}\right) \tag{2a}$$

or more conveniently

$$\frac{z_1}{r_B} = 0.0275\left(\frac{D_t}{d_B}\right)^3. \tag{2b}$$

Some further complications in the modeling of z_1 will be evaluated in the Discussion section.

The relationship between a crater's size and the depth provenance of its ejecta is an issue that transcends the narrow context of modeling megaregolith development. Planetary petrologists, especially lunar petrologists, often ponder the depth provenance of materials excavated by impact (e.g., Wilhelms 1987; Warren 2001b; Haskin et al. 2003). Yet the relationship between D and the statistical depth provenance of a crater's ejecta has never, to my knowledge, been described in a detailed manner. This relationship was, implicitly, constrained long ago by Maxwell's (1977) excavation model. For translating Maxwell's (1977) model into the desired statistical assessment of the depth provenance of a crater's ejecta, the first step is to calculate the depth of excavation ω along the basal streamline, i.e., the streamline that intersects the ground level at $r = R_t$. Croft (1980) showed that this streamline can be expressed by the following rectangular coordinates:

$$r = R_t \sin\theta\,(1 - \cos\theta)^{1/(Z-2)} \tag{3a}$$

$$\omega = R_t \cos\theta\,(1 - \cos\theta)^{1/(Z-2)}, \tag{3b}$$

where θ is the angle between a vertical line extending down from the point of impact and the streamline at the given r (e.g., with $Z = 2.734$ the maximum excavation depth ω_{max} of $0.2R_t$ occurs at $\theta = 65°$ and $r = 0.429R_t$; at $\theta = 90°$, $r = R_t$ and $\omega = 0$). The resultant shape model can be converted into a depth-provenance spectrum by numerical integration, i.e., by counting the number of cells at a given depth when the ejection zone is modeled as a 3-D grid space. In practice, instead of a fully 3-D model, I employed a 2-D model with r^2 weighting of the cell volumes. Adequate resolution was achieved using 0.5° increments for θ and $0.001D_t$ vertical increments. Results are shown in Fig. 4. The curve shown assumes $Z = 2.734$ (i.e., depth/

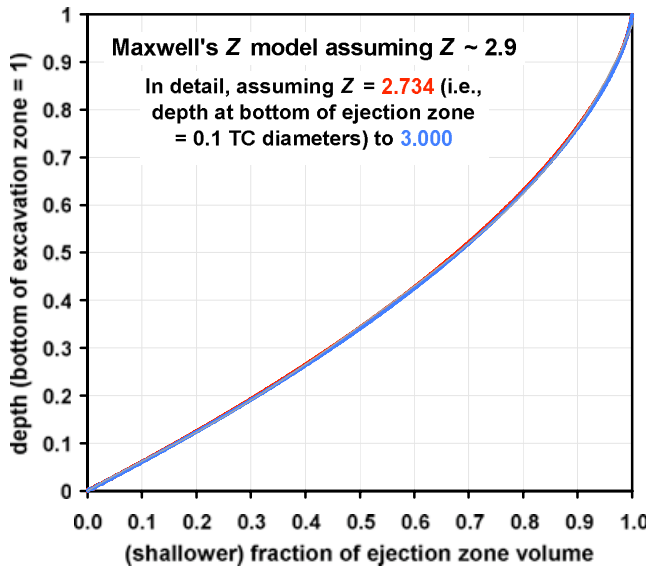

Fig. 4. Depth provenance for ejecta from an individual crater, as implied by Maxwell's (1977) Z-model assuming $Z \sim 2.9$ (a depth/diameter ratio for the excavation zone of precisely 0.1 implies $Z = 2.734$; however, as explained in the text, the precise choice of Z is not important for this diagram).

diameter of the ejection zone = 0.10). Note that as a consequence of the curve's concavity, only 32 vol% of the ejection zone is deeper than the depth of 0.5 (times the maximum), 11 vol% is deeper than the depth of 0.75, etc. For $Z = 3.00$ ($\omega_{max} = 0.25R_t$), the curve becomes slightly more concave, but the difference in terms of Fig. 4 would be almost imperceptible.

Populations of Craters

The anchor point for this model is the observed or assumed largest crater, whose transient crater diameter (of course, never precisely observable) is D_L. The size–frequency distribution of the rest of the population, on an average or typical body, is conventionally modeled by a power law:

$$N_{cum}(D) = cD^{-b}, \quad (4)$$

where N_{cum} is the cumulative number of craters with diameter D or larger, and in the ideal case of a single b applying to the entire size spectrum, $c = 1/D_L{}^{-b}$. This power law is usually applied to final crater rim diameters, but its form is equally germane to transient craters. Assuming the excavation crater shape is size independent, a b of 3 implies that the volume of excavation is size independent, i.e., every size interval contributes an equal fraction of the total cumulative ejecta volume. A b of 2 implies that the surface coverage of craters is size independent, i.e., craters in every size interval represent the same areal fraction of the total surface, while the relative volume of cumulative cratering-excavation is proportional to D. A physically implausible b of 1 would imply that all but the largest few craters contribute negligible ejecta volume. For any given D_L as anchor point, the smaller b is, the thinner the final accumulation of ejecta will be.

As indicated by, e.g., Holsapple (2003), in the small-scale "strength" regime at any given impact velocity v_i (and an impact angle not extremely far from 45°) the transient crater diameter D_t will be in approximately fixed proportion to the impactor diameter d_i; e.g., if $v_i = 5$ km s^{-1} (the typical asteroid–asteroid encounter velocity), D_t will be $\approx 10d_i$. As the influence of gravity g increases for very large craters, the D_t/d_i ratio tends to decrease. Still, we can constrain the b of the crater size power law (Equation 4) indirectly by constraining the exponent β for the analogous impactor-size power law: $N_{cum}(d) = cd^{-\beta}$. In general, 2.5 is the canonical value for β in a population that undergoes collision-fragmental selection (Dohnanyi 1969). But the present-day asteroid population shows a complex distribution (e.g., Asphaug 2009), probably as a result of various size dependent, especially g-related, effects. Bottke et al. (2005a; cf. O'Brien and Greenberg 2005) inferred that this population, although greatly reduced in numbers, probably has a size–frequency distribution similar in shape to the population during the late stages of major accretion. In this distribution, β is approximately 2.1 overall, but 1.94 for the d range of 1–50 km, approximately 1.63 for the range of 50–100 km, and it increases toward 3 for $d > 100$ km. The details of the size distribution have implications that are best evaluated after an assessment of constraints on D_L.

For bodies of the relevant size range ($d_B > 100$ km), observational constraints on D_L/d_B are in short supply. As reviewed by Leliwa-Kopystyński et al. (2008), the data set for asteroids and satellites (other than the Moon) includes only one body known to combine rocky mineralogy, $d_B > 53$ km, and a well-determined largest crater size: Vesta, with $d_B \sim 530$ km and $D_L/d_B \sim 0.58$ (Leliwa-Kopystyński et al. indicate a value of 1.739 for what they call "D/R," but this ratio involves the diameter of the largest final observed crater, not, as with D_L/d_B, the largest inferred transient crater). Bodies with $d_B << 100$ km are not only irrelevant; their largest observable craters probably tend to be much smaller than their true largest craters. Asphaug (2008) noted that impact-seismic shaking effectively smoothes the surfaces of smaller bodies, and inferred that the size dependency of this process accounts for a correlation between apparent D_L/d_B and d_B. Resurfacing can also be a problem with larger bodies. Vesta and the Moon were probably hot enough for long enough (a "magma ocean" is often invoked for

both) that some of the largest impacts left no manifestation on the present surfaces.

Dynamical models indicate that in general, especially during the late stage of accretion (~2 Ma after its onset) when encounter velocities began to approach modern values even as multi–hundred-kilometer planetesimals became common (Weidenschilling and Cuzzi 2006), which incidentally was at about the same time heat build-up from ^{26}Al climaxed (Hevey and Sanders 2006), planetesimals probably had to endure impacts energetic enough to challenge their ability to survive. Beyond some impact-energy limit, ejected matter begins to escape more than it lands. As for any given target-body size the transient crater diameter D_t scales as the cube root of impact energy, the transition from growth to catastrophic disruption is quite abrupt, in terms of D_L/d_B. Thus, unless b is much less than 2, D_L is probably within a few tens of percent of the catastrophic-disruption crater diameter D_C (expressed in this work, like D_L, in terms of the transient crater diameter).

Housen et al. (1979) estimated that D_C is of order 1/3 to 2/3 of d_B, depending on the size and mechanical strength of the target body. By contrast, Nolan et al. (2001) suggested that shock-induced fracture in advance of crater excavation flow reduces the potential for catastrophic mass loss, which results in a D_C/d_B ratio of 1.3 for even a small asteroid (Gaspra, d_B modeled as 12.6 km) being impacted at 5 km s^{-1}. As suggested by Bottke et al. (2005a, 2005b), the disruption threshold can be modeled in terms of d_C, the diameter of the catastrophic impactor:

$$\frac{d_C}{d_B} = \left(\frac{2Q_C}{v_i^2}\right)^{(1/3)}, \quad (5)$$

where Q_C is the critical specific impact energy (units of J kg^{-1}). Q_C is hard to constrain, especially for small bodies, which undergo strength-regime cratering. But for bodies greater than about 10 km in diameter, several different approaches (see reviews in O'Brien and Greenberg 2005; and Asphaug 2009) suggest a relationship not far from that shown in fig. 5 (curve "10") of Bottke et al. (2005b), which implies

$$Q_C = 0.318 d_B^{1.348}. \quad (6)$$

The d_C/d_B implied by Equation 5 scales as $v_i^{-(2/3)}$. At the modern prevailing asteroid-asteroid encounter velocity of 5 km s^{-1}, $d_C/d_B = 0.024 d_B^{0.45}$ (for d_B in km), and thus d_C/d_B ranges from 0.07 to 0.53 for d_B = 10–1000 km. At a late-accretionary v_i of say 2 km s^{-1}, these d_C/d_B predictions shift to 0.12 and 0.99, respectively. Figure 5 shows the d_C/d_B implied by Equation 5 translated into the critical impactor mass ratio m_C/m_B. Figure 5 also shows for comparison m_C/m_B as implied by the "best fit" $Q_C(d_B)$ relationship of O'Brien and Greenberg (2005) which, as reviewed by those authors, is, for the d_B range of interest, lower than most other estimates by a factor that is fairly representative (i.e., roughly 1σ below Bottke's Q_C) of the overall scatter among such estimates in recent literature. In other words, the nominal uncertainty in m_C/m_B is approximately a factor of 2.

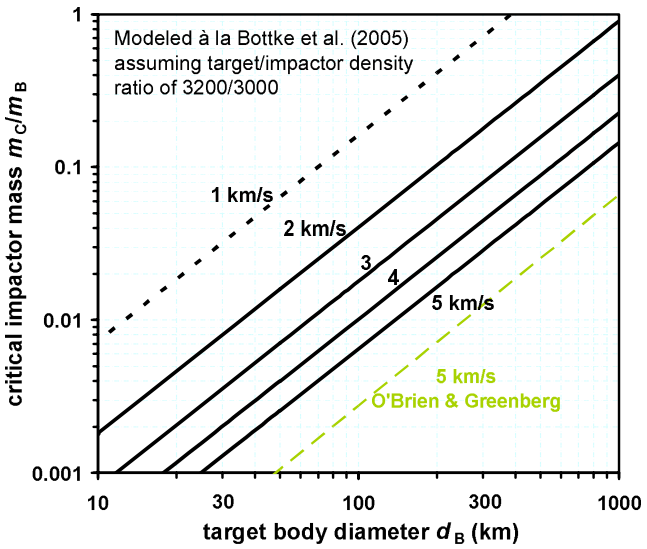

Fig. 5. The critical impactor mass for catastrophic-disruption m_C, expressed as the ratio m_C/m_B, calculated as a function of target-body diameter d_B for a range of impact velocities, by extension of the Q_C model of Bottke et al. (2005a, 2005b). Also shown for comparison is the 5 km s^{-1} m_C/m_B implied by the lower Q_C estimate of O'Brien and Greenberg (2005).

For translating between d_C/d_B and the catastrophic-destruction crater diameter ratio D_C/d_B (and more generally between d_i/d_B and D_t/d_B), I developed parameterizations (i.e., a series of polynomial fits) of D_t results for various combinations of d_i and d_B using Holsapple's (2003) implementation of π-scaling for crater dimensions. Additional inputs were an impact angle of 45°; rocky physical characteristics for both impactor and target, i.e., densities of 3000 and 3200 kg m^{-3}, respectively; and g and escape velocity calculated as a function of d_B under the assumption of uniform density ρ within the target; i.e., $g = (4/3)\pi G \rho_B r_B$ and $v_{esc} = (2Gm_B/r_B)^{1/2}$. π-Scaling indicates that for impact velocity v_i of 5 km s^{-1} the D_t/d_i ratio is uniformly close to 10 in even the largest of craters on a d_B << 100 km body, but decreases to, e.g.,

7.4, 5.4, 3.7, 2.5 in $D_t/d_B \sim 1.0$ events for d_B = 100, 200, 400, and 800 km, respectively.

Under the assumption that accretion was oligarchical (not runaway), so that the asteroids and planetesimals are/were stochastic survivors from a series of near-catastrophic collisions, Poisson statistics and the power-law size distribution, $N_{cum}(d) = cd^{-\beta}$, can be applied to estimate the probability of d_L being smaller than d_C by a given factor. The Poisson equation for probability of zero outcomes is simply $p_0 = e^{-n}$, where n is the number expected from ideal sampling of the overall population. By this method (Fig. 6; with relative d translated into relative mass assuming simple d^3 proportionality), for $\beta \sim 2$, the most likely outcome is $m_L/m_C \sim 0.45$. This result varies as a function of β; a m_L/m_C range of 0.35–0.59 is implied by varying β from 1.5 to 3. Figure 7 shows the D_L/d_B ratios that result from assuming m_L/m_C = 0.25–0.75. As a rule of thumb, for bodies of the size range under consideration, $m_L/m_C \sim 0.5$ translates into $D_L/d_B \sim 1.0$.

Returning to the problem of constraining b, the $\beta(d_i)$ of the asteroidal size distribution (Fig. 1) (Bottke et al. 2005a) can be translated into a $\beta(m_i/m_C)$, by using Equation 5 to derive d_C, and thus m_C, for any given target-body size and impact velocity. Since β is a measure of slope, seemingly small bumps and dips on the size distribution become magnified, so that results (Fig. 8) for large m_i/m_C in the relevant d_B range are remarkably structured, with a peak at approximately 80 km and $\beta \sim 2.5$, a deep valley at approximately 220 km and $\beta \sim 1.3$, and then a gradual rise toward approximately 800 km and $\beta \sim 3$. One complication is that gravity's effect of limiting the growth of large craters causes the ratio D_t/d_i to decrease (for any given v_i) with increasing d_i, so the size–frequency exponent b for transient crater diameters is slightly greater than the corresponding β for impactor diameters (i.e., the distribution's slope, for large, high-g bodies, is mildly but systematically steeper). I have not attempted to model the minor increase between β and the corresponding b, except by taking $m_L/m_C \sim 0.5$, and $D_L/d_B \sim 1.0$ (rather than 0.45 and ~0.9), as the most likely outcome implied by the Poisson-statistical approach at the end of the previous paragraph.

Another complication is that in late-accretionary times the prevailing v_i was lower. Weidenschilling and Cuzzi (2006) estimate that even after 2 Ma of accretion, typical impact velocities were still "a few tenths to approximately 1 km s^{-1}." The implied impactor diameter d_i to yield a given crater D_t scales as $1/v_i^{0.5}$. A lower v_i shifts the β spectrum's features to smaller d_B; e.g., with v_i, = 2.5 km s^{-1}, the $\beta \sim 1.3$ valley shifts to approximately 160 km, and the two peaks shift to approximately 75 and 400 km.

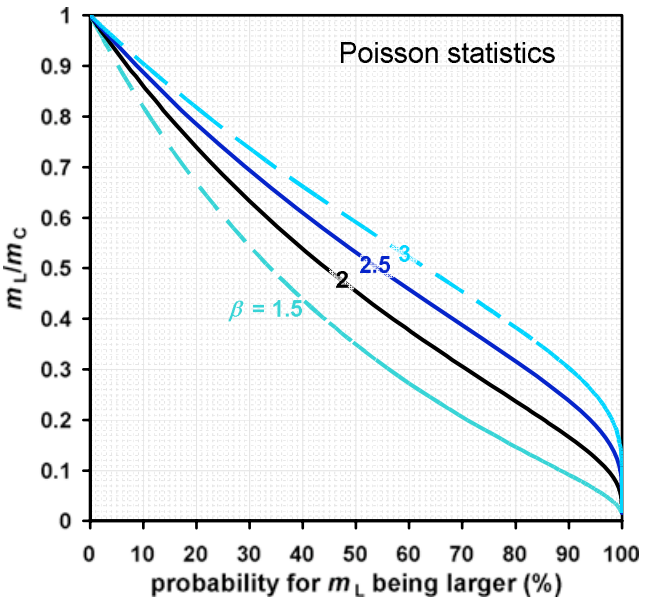

Fig. 6. Poisson-statistical probability for the largest mass of impactor m_L in terms of m_L/m_C ratio, assuming that the body is a fortunate survivor among many that have been catastrophically disrupted, and that the population of impactors conforms to the power-law size distribution with slope β (the β shown refers to the diameters of the impactors, albeit this chart shows diameter translated into mass).

In summary, D_L/d_B is unlikely to be much less than 1. For the near-largest impacts, $b \sim 2$ is probably conservatively low as a single value to represent the general populations of craters and target bodies considered in this work. For many of the largest craters on the largest bodies, particularly if the cratering occurred mostly during the late stages of accretion while the prevailing v_i was increasing but still much less than 5 km s^{-1}, b may have been closer to 3.

Modeling Ejecta Accumulation

For modeling purposes, the entire volume of the excavation/ejection zone is assumed to accumulate upon the surface of the target body (obviously this is not strictly correct, but it is justified as a simplification in the next section). The statistical crater size distribution is modeled per Equation 4, for which the only input, other than D_L, is b. The statistical accumulated average thickness z_A can be calculated by summing the individual ejecta volumes of all craters, starting from D_L, down to a size where the incremental increase in global ejecta layer thickness becomes insignificant. Models were constructed to include the largest 2^{16} (65,536) craters on the body. This number is overkill for models assuming that b is 3 or less. The only complication is that for each impact, the potential

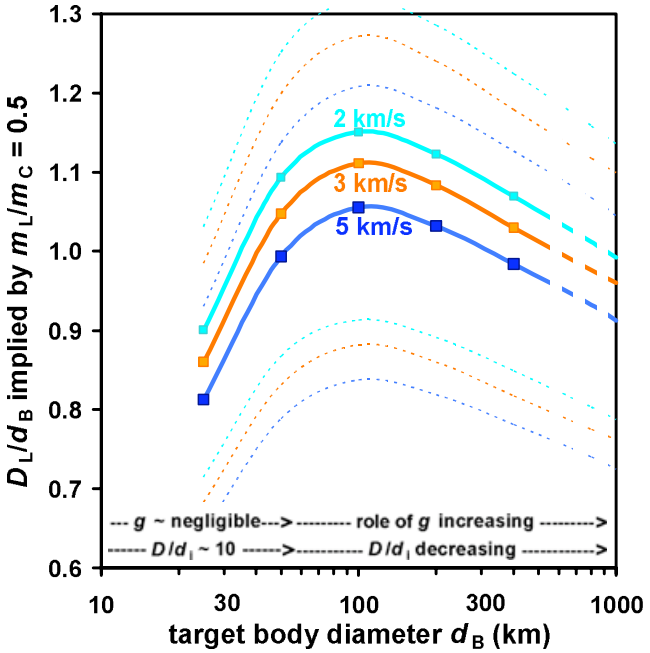

Fig. 7. The largest (transient) crater D_L/d_B, calculated as a function of target-body diameter d_B assuming that the largest crater is formed with m_L/m_C = 0.5; i.e., the impactor mass m_L is 50% as massive as the catastrophic-disruption mass m_C, as calculated by extension of the model of Bottke et al. (2005a, 2005b). Translation from that mass m_L of the largest impactor into (for an assumed impact velocity) its D_L is modeled based on Holsapple (2003), assuming "rock" impacts into "hard rock" targets (for further description, see text) at 45° and the indicated velocity. Light-dashed curves show results assuming m_L/m_C = 0.25–0.75.

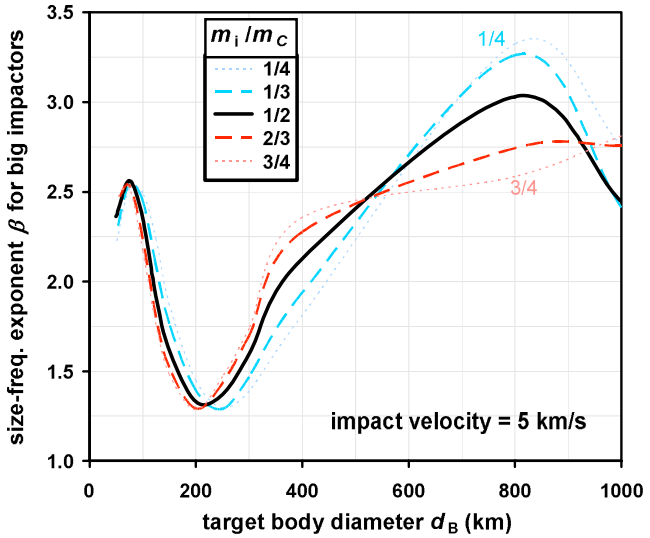

Fig. 8. The size–frequency exponent β implied by the modern asteroids (Bottke et al. 2005a) shown in relation to the target-body diameter d_B and five values of the impactor mass ratio, m_i/m_C, i.e., the mass of an impactor ratioed to the catastrophic-disruption impactor mass (at v_i of 5 km s^{-1}) for the given d_B.

contribution of new ejecta, per Equation 2, is reduced by the fraction ζ of the crater's ejecta that is "recycled" from depths within the preexisting global ejecta layer. The magnitude of ζ is constrained as the fraction of the excavated volume that, per a precise fifth-order polynomial fit to the trend in Fig. 4 with the maximum depth of excavation ω_{max} assumed = $0.1D_t$, is shallower than z_A. The Fig. 4 results were parameterized as:

$$\zeta = -0.193\eta^5 + 0.312\eta^4 - 0.191\eta^3 - 0.608\eta^2 + 1.680\eta, \quad (7)$$

where η is the ratio z_A/ω_{max}. Here, z_A is the value immediately prior to the impact being evaluated; and both z_A and ω_{max} are treated in units of (i.e., normalized to) r_B, the radius of the target body. Of course, for any crater with $\omega_{max} < z_A$, the ejecta is 100% recycled and no new growth of z_A occurs.

Figure 9 shows the final results from this model: average accumulated ejecta layer thickness z_A (in units of r_B, after all 2^{16} craters form) as a function of assumed D_L/d_B ratio. The sequence of crater formation, although potentially marginally significant, is not crucial. The four main curves in the figure are each based on a set of 10 randomized sequences of formation for the 2^{16} craters. But as the two light-dashed curves indicate, even under the extreme assumption that the craters form in a sequence of size (either smallest to largest or largest to smallest), results are only marginally different from the average randomized-sequence result. The crater-formation sequence is slightly consequential for models assuming a high b; e.g., for b = 3 and D_L/d_B in the range 0.4–1.0, z_A could in principle vary, between the extremes of the decreasing crater size model and the increasing crater size model, over a factor of 1.4. Figure 10 shows the same model results translated, by straightforward conversion from units of r_B for z_A into units of kilometers, for a range of different target-body diameters.

In Fig. 11, the same results (Figs. 9 and 10) have been recast with the largest impactor mass ratio m_L/m_B taking the place of D_L/d_B for the x-axis. Masses were derived from diameters assuming the same densities as employed in the modeling of D_t/d_i, i.e., Holsapple's (2003) "rocky" densities. An interesting effect follows from the decrease in D_t/d_i (for any given v_i) with increasing d_B. By Equation 2b, ejecta yield (z_1/r_B) scales as the cube of D_t/d_B. Thus, the factor by which D_t/d_i decreases with increasing d_B (Holsapple 2003) gets cubed in the evolution of z_A. The net effect is that even though the modeling implies a uniform ejecta accumulation z_A/r_B ratio for any given D_L/d_B (Fig. 9), in terms of absolute thickness (in kilometers) z_A remains

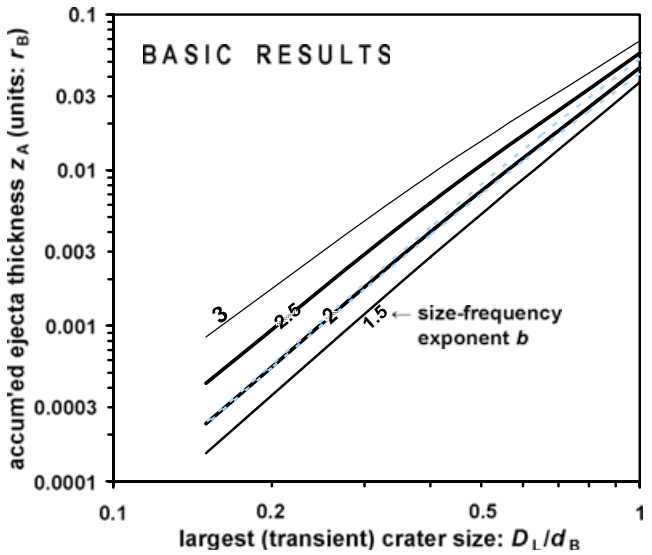

Fig. 9. Results for relative thickness of the global ejecta accumulation z_A as a function of the size of the largest crater (D_L) and the crater size–frequency exponent (b). The heavy-continuous curves represent averages from 10 different models (for each b value in the sequence 1.5, 1.75, 2, 2.25 . . . 3), each with 65,000 model craters forming in a different random sequence. The thin-dashed curves indicate, for the $b = 2$ model, results based on extreme variants of crater-formation order: The curve on the high-z_A side of the main, random-order curve represents a model with craters forming (implausibly) in sequence from small to large; the curve on the low-z_A side of the main, random-order curve is based craters forming (implausibly) in sequence from large to small.

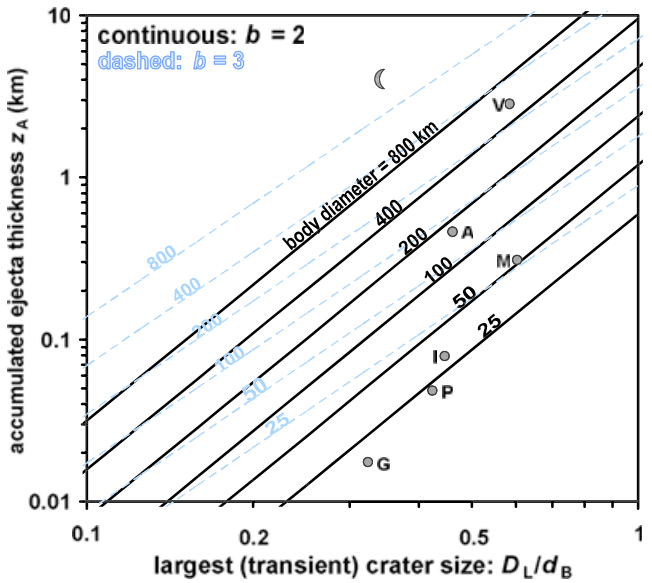

Fig. 10. Global ejecta accumulation thickness z_A expressed in kilometers, as a function of the size of the largest crater (D_L) and two different assumed values for the crater size–frequency exponent (b), as calculated for a range of target-body diameter d_B. These results were derived from the same averaging of ten 65,000-crater models as described for Fig. 3. Assumptions include target body consisting of Holsapple's "hard rock" ($\rho_B = 3200$ kg m^{-3}), impactor 3000 kg m^{-3} hitting at v_i of approximately 5 km s^{-1} and 45° impact angle. Also shown on the assumption that $b = 2$ are the sizes of the largest craters on asteroids Vesta (V), Amalthea (A), Mathilde (M), Ida (I), and Gaspra (G), along with the Moon (crescent symbol) and Phobos (P), as compiled by Asphaug (2008). The Moon is plotted under the assumption that its largest impact basin is South Pole-Aitken, 2500 km in d. Under the hypothesis that Procellarum Basin is also an impact structure whose rim (or main ring) is 3200 km in diameter (Wilhelms 1987), the Moon's D_L/d_B would shift to approximately 0.42.

relatively constant for any given d_L/d_B (or m_L/m_B) over a huge range in d_B (Fig. 11). Readers with an interest in specific target-body sizes (and trusting the Bottke et al. 2005a model for Q_C plus their argument that the size–frequency distribution of planetesimals is closely mirrored by the present-day asteroids) may want to fine-tune these results based on the β variations shown in Fig. 8.

Assuming that the largest event involves a m_L that is a large fraction of m_C as calculated by the (extended) Bottke et al.'s (2005a, 2005b) model (Fig. 5; for impact velocity v_i of 5 km s^{-1}), we arrive at a simple plot of body diameter d_B versus expected thickness z_A of accumulated ejecta (Fig. 12). Within the overall uncertainty of the modeling, the relationship is essentially linear at $z_A/d_B \sim 0.04(m_L/m_C)$ (valid for $m_L/m_C \sim 0.25$–0.75).

As illustrated in Fig. 13, the single biggest crater typically contributes a large fraction of the total ejecta accumulation, especially in cases of low b combined with a high D_L/d_B ratio. Consider, for the nominal b of 2, the case of a largest crater with D_L/d_B similar to the D_t/d_B of Vesta's great southern basin, approximately 0.58 (Vesta's $d_B \sim 530$ km, and per Asphaug 1997, Holsapple 2003, etc., the D_{rim} of approximately 460 km implies $D_t \sim 310$ km). This one crater will produce on average (depending, inter alia, on when it forms relative to other large craters) approximately 40% of the body's total accumulation of otherwise unexcavated ejecta. However, in terms of the present surface layer about to be studied by Dawn (Russell et al. 2004), the basin's ejecta probably so greatly churned the surface upon landing at distal locations (cf. Haskin et al. 2003) that the basin does not necessarily dominate the mix of surface debris except within $\sim 2R_t$ ($\sim$300 km) of its rim.

Some caveats are in order. Realistically, for bodies near the smaller (100 km) end of the size range under consideration, d_C is probably sensitive to the material properties of the target body, which means that the true uncertainty in m_C, as derived by extension of Bottke et al.'s (2005a, 2005b) model for Q_C and d_C/d_B, is hard to even estimate. Moreover, for bodies other than growing planetesimals there is no assurance that

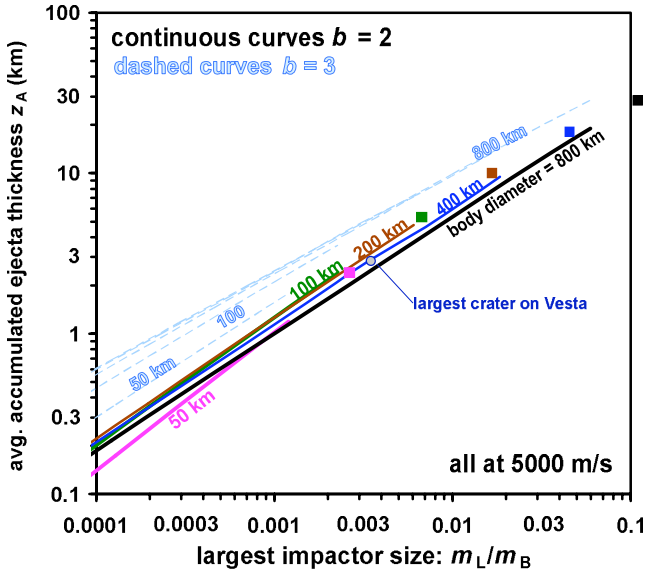

Fig. 11. Global ejecta accumulation thickness z_A expressed in kilometers, as a function of the mass of the largest impactor (m_L) and two different assumed values for the crater size–frequency exponent (b), as calculated for a range of target-body diameter d_B. These results were derived from the same averaging of ten 65,000-crater models as described for Figs. 8 and 9. Five color-filled squares indicate (for $b = 2$ curves) the catastrophic-disruption mass m_C/m_B as estimated using the Bottke et al. (2005a, 2005b) approach (Fig. 5; assuming $v_i = 5$ km s^{-1}). Assumptions include target body consisting of Holsapple's "hard rock" ($\rho_B = 3200$ kg m^{-3}), impactor 3000 kg m^{-3} hitting at v_i of approximately 5 km s^{-1} and 45° impact angle.

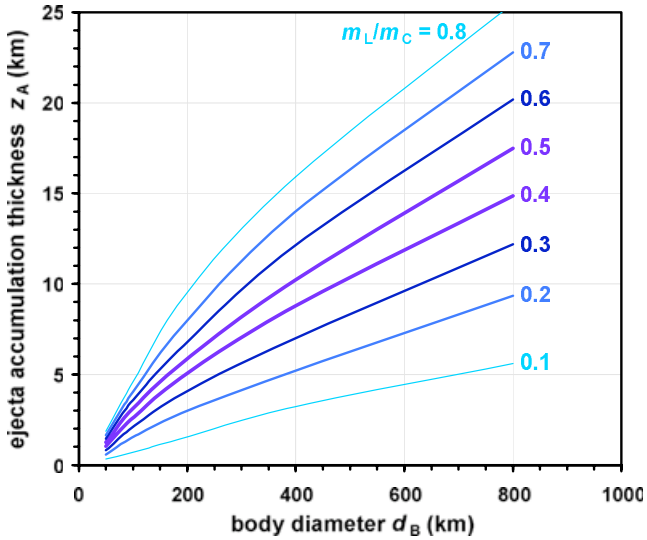

Fig. 12. Results for the mean global ejecta accumulation thickness z_A for a growing planetesimal as a function of the diameter of the body, shown for $b = 2$ and a range of assumed values for mass of the largest impactor m_L in relation to the catastrophic-disruption mass m_C; with m_C estimated using the approach of Bottke et al. (2005a, 2005b) for $v_i = 5$ km s^{-1}.

m_L would bear a strong relationship to m_C. If Bottke et al.'s (2005a, 2005b) model for estimating d_C/d_B were applied to the Moon, the predicted diameter of a catastrophic impactor (assuming $v_i = 20$ km s^{-1}) would be approximately 1270 km. For comparison, the biggest definite lunar impact basin, South Pole-Aitken ($D_t \sim 1100$ km), probably formed from an impactor with d_i of roughly 300 km (Holsapple 2003; of course, the Moon's size and origin as a natural satellite probably led to an unusually prolonged history of resurfacing by igneous activity, in comparison to most planetesimals). The accuracy of the model probably diminishes (most likely tending to underestimate z_A; see next section) as D_L/d_B increases past approximately 1. For a planetesimal evolving during the middle-late stages of accretion, when encounter velocities are still of order 2–3 km s^{-1}, m_C/m_B is approximately four times greater, $d_C/d_B \sim 1.6$ times greater, and $D_C/d_B \sim 1.07$ times greater than the 5 km s^{-1} ratios (Figs. 5 and 7); and as a consequence of the higher D_C/d_B, for any given m_L/m_C scenario, the implied total volume of ejecta is $1.07^3 = 1.23$ times greater than in the nominal 5 km s^{-1} model. Finally, if ever the ejecta is subjected to significant sintering-densification (see below), z_A becomes an upper limit for megaregolith thickness.

Additional Single-Crater Complexities

Equation 2 implicitly assumes that the volume of the ejection/excavation zone is identical to the volume of the ejecta in its final state as debris strewn (mostly) onto the surface of the body (the stipulation sometimes called "Schröter's Rule"). Here, two significant but offsetting aspects of approximation are involved. First, to the extent that the final debris is in general more porous and thus of higher volume than the preimpact material, Equation 2 tends to underestimate z_1. However, particularly on smaller bodies, a significant fraction of the ejecta may not land at all, and in that sense Equation 2 tends toward overestimation of z_1. One way to gauge the magnitude of this effect is to apply the comprehensive crater scaling model of Holsapple (2003), which estimates the mass–velocity spectrum for the ejecta, with g and escape velocity (which scales approximately as d_B^1) among the input parameters. As summarized in Fig. 14, the fraction of ejecta launched off the body is in general roughly offset by the porosity-inflation factor (assumed to be ~5/4). In actuality, the porosity of the ejecta accumulation probably anticorrelates with d_B (i.e., with g, which

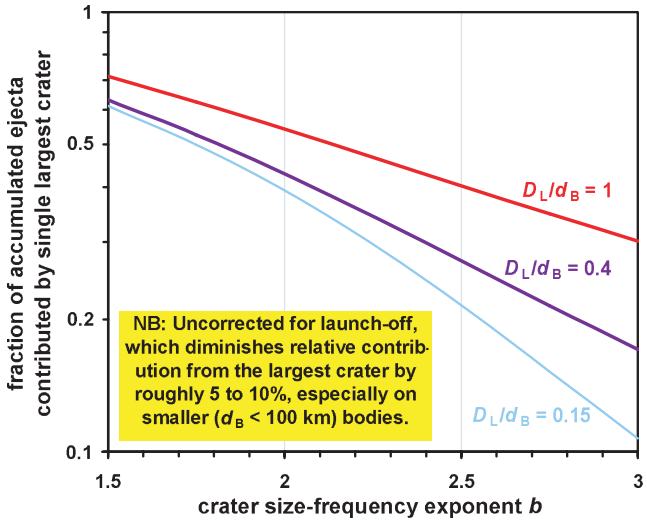

Fig. 13. Fraction of accumulated ejecta contributed by the single largest crater, shown as a function of b for three different values of D_L/d_B (the three corresponding approximate m_L/m_B ratios for impacts at 5 km s^{-1} into a 100 km [d_B] "rocky" target body are 3.6×10^{-6}, 9×10^{-5}, and 2.3×10^{-3}). These results were derived from the same averaging of 65,000-crater models, with the craters formed in 10 different randomized sequences, as described for Fig. 8. As noted in the figure, these results are *not* corrected for the greater proportion of launch-off associated with large events, especially important for small bodies.

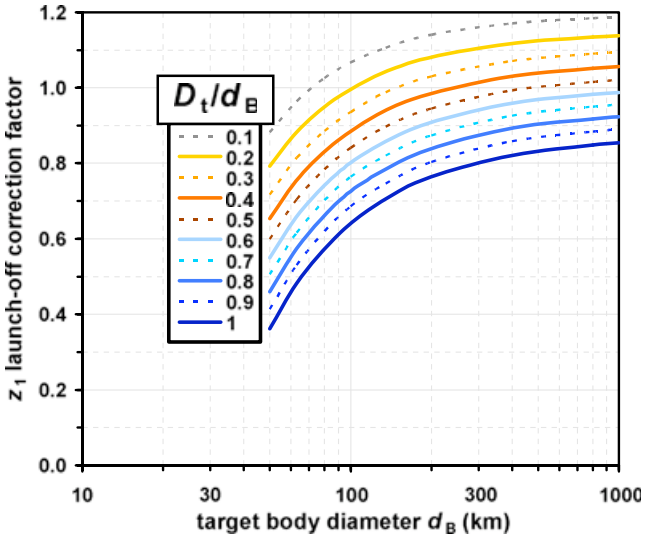

Fig. 14. The proportion of the ejecta lost by off-launch as constrained by π-group scaling (Holsapple 2003), shown as a "correction factor" for the implied final volume of the landed ejecta, as a function of transient crater diameter D_t and target-body diameter d_B. The correction consists of multiplying z_1 times the fraction of ejecta that lands (i.e., does not undergo launch-off) times a factor of 5/4 as (approximate) correction for increased porosity in comparison to the target material. Assumptions include target body consisting of Holsapple's "hard rock" (ρ_B = 3200 kg m^{-3}), v_i of order km s^{-1} (the calculations were done assuming 5 km s^{-1}), and 45° impact angle.

drives compaction). Other factors, nonspheroidal shape and the typically fast asteroidal rotation rate, probably slightly increase the launch-off proportion (Geissler et al. 1996). The modeling used for Fig. 14 conservatively assumes "rocky" strength for the target body. π-Group scaling (Holsapple 2003) indicates that for a given crater size, a stronger target results in a higher proportion of ejecta loss by launch-off. As an extreme example, during formation of a 5 km D_t on a small (d_B of order 10 km) asteroid, the proportion of launch-off is five times greater if the target is a strong "rocky" material than if it has strength equivalent to the powdery lunar surface regolith. (The mass of launch-off is about two times greater in the weak target for a given impactor mass, but the crater that forms, and the total volume of ejecta, is vastly larger in the weak target.) In terms of thermal-insulation implications, invoking a weakly cohesive target effectively preempts the megaregolith thickness issue, because weakly cohesive material will almost inevitably (in the context of atmosphereless bodies) be material rich in vacuous porosity, and thus constitute insulation equivalent to megaregolith even if it not formed mainly by aggregation of crater ejecta. In summary, simple application of Equation 2 may overestimate z_A, but probably not by an important factor unless d_B is < 100 km.

The Equation 2 model for z_1 does not agree well with results reported from hydrocode experiments by Nolan et al. (2001) for very large impacts on Gaspra, modeled as a sphere with $d_B \sim 12.6$ km. Nolan et al. (2001) (their fig. 5) found $z_1 \sim 16$ m from formation of a single crater with $D \sim 4.6$ km. In their model, some unspecified proportion of the ejecta is lost due to launch-off (however, the launch-off loss was probably low for this, the smallest crater they considered). By contrast, Equation 2, assuming no ejecta loss by launch-off and that by "crater diameter" Nolan et al. (2001) meant D_t (and not a larger final D), implies for the 4.6 km crater a z_1 of only 4.3 m: a discrepancy of a factor of 3.7. A log-linear trend that Nolan et al. (2001) drew through their results indicates that a 3 km crater forms a z_1 of 13 m, which implies discrepancy relative to Equation 2 by a factor of 11. This discrepancy calls into question an inference by Nolan et al. (2001) that net ejecta deposition is "approximately linear in impactor size . . . due to a combination of crater volume and fraction escaping" for large impacts. (Perhaps, despite other contextual indications, by "size" Nolan et al. 2001 meant mass.)

A complication not modeled by Equation 2 may arise in cases where the D_t/d_B ratio approaches or

exceeds 1. A D_t/d_B of approximately 1 implies that the transient crater spans approximately 32% of the body's circumference. In such a case, as Cintala et al. (1978) pointed out, the crater's depth/diameter ratio (if depth is defined relative to the preimpact surface, not to a chord across the crater rim) may increase markedly. Hydrocode modeling by Hammond et al. (2009; cf. fig. 2 in Nolan et al. 2001) indicates that the maximum excavation depth ω_{max} is approximately 0.17 ± 0.03 times D_t in giant ($D_t/d_B \sim 0.2$–0.7) approximately 20 km s^{-1} lunar impacts. However, they also found that the ω_{max}/D_t ratio moderates at lower impact velocities; so the general implications of Hammond et al. (2009) for ω_{max}/D_t and the volume of ejecta z_1 are hard to gauge. However, if the giant impacts do excavate much deeper than 0.1 times D_t, they probably excavate higher proportions of "new" (as opposed to recycled) megaregolith than Equations 3*a* and 3*b* imply. Comparison with the uppermost light-dashed curve in Fig. 9 (i.e., the ideal case of zero recycling) indicates that in scenarios where D_L/d_B exceeds approximately 1, the nominal model may underestimate the total ejecta accumulation z_A by 10–20%.

Other complications not modeled by Equation 2 include: megaregolith destruction by compaction directly below the crater; the effects of secondary cratering (as the ejecta land, with compaction versus churning depending on, inter alia, the ejecta velocity); growth of the body (and thus its surface area) during accretion; and the transformation of a fraction of the ejecta into melt and even vapor. However, if the Moon is any guide, even impact-melt dominated ejecta tend to solidify into moderately porous, thermally insulating rock types (Fig. 1).

DISCUSSION

Temperature Dependence of *k*

The conductivities shown in Fig. 1 are for 300 K, but temperatures within a megaregolith on a hot planetesimal or asteroid may extend from near 250 K at its surface to, near its base, the sintering T of roughly (see below) 1000 K. At low-moderate T the lattice-vibration component of thermal conductivity surely predominates, but the radiative component k_{rad} is T-sensitive and insensitive to porosity. Early studies (Schatz and Simmons 1972; Shankland et al. 1979) indicated a large dk_{rad}/dT for olivine (which probably dominates the shallow interior of any not-yet extensively differentiated planetesimal or asteroid), such that k_{rad} would reach, for typical mantle grain sizes, approximately 1.2 W m^{-1} K^{-1} at 1000 K. If this were accurate, the implication would be that regardless of porosity, a megaregolith's k becomes rocklike as T approaches sintering. However, according to Hofmeister (1999, 2005), the early dk_{rad}/dT estimates were grossly inaccurate, and olivine's k_{rad} only increases to approximately 0.2 W m^{-1} K^{-1} at 1000 K. Hofmeister (2005) also found that the Fa content of olivine has little influence on k_{rad}. The deep megaregolith's k is probably moderated more by sintering-enhanced compaction, and by its relative immunity to gardening-pulverization (i.e., involvement in small cratering events), than it is by dk_{rad}/dT.

Uneven Ejecta Deposition

Even in the low-*g*, high-surface-curvature, high spin-rate environment of a planetesimal or asteroid, ejecta probably land mostly within 2–3 radii of the (transient) crater's rim (e.g., Nolan et al. 2001). Uneven megaregolith accumulation might be a significant limitation on the effectiveness of the megaregolith as a thermal-insulation blanket. However, barring a flukish exception to the power-law model of size–frequency distribution, the biggest crater will usually be accompanied by a considerable number of comparably large craters formed at scattered random locations. If $b = 2$, with average sampling and including craters formed both before and after the D_L event, there will be three more craters with $D_t \geq 0.5D_L$, and an additional 12 with $0.25D_L \leq D_t \leq 0.5D_L$. Even if b is as low as 1.5, with average sampling there will be three more craters with $D_t \geq 0.4D_L$, and an additional seven with $0.2D_L \leq D_t \leq 0.4D_L$. If $b = 2.5$, with average sampling there will be a total of 10 craters with $D_t \geq 0.4D_L$. Divide these numbers by 2 to arrive at the numbers that on average will form at a later date than the D_L crater. Areas that avoid ever being within a few radii of any major crater are probably minor. In terms of thermal implications, a moderating factor is that such a surface would generally at least undergo extensive gardening by small craters (i.e., develop a regolith; see The Regolith Within the Megaregolith section below), so its megaregolith, although thin, will tend to be more porous and have a lower conductivity than the global average megaregolith.

The Bottke et al. (2005a, 2005b) model for relationships among d_C/d_B, Q_C, and v_i implies that big D_t/d_B craters are likely to be more widely scattered (in relative terms) on small-d_B bodies, with their low D_C/d_B (Fig. 5) and thus low D_L/d_B. However, on smaller bodies both seismic shaking (Cintala et al. 1979; Asphaug 2008), and a momentum-transfer process that Nolan et al. (2001) call impact "jolting," may lead to enhanced dispersal of the landed ejecta.

Very Large Ejecta

Ejecta that remain in the form of large intact fragments are in general much less porous, and more thermally conductive, than accumulations of finely pulverized ejecta. The classic fragmentation model (Dohnanyi 1969) produces a power-law size spectrum analogous to Equation 4 with $\beta \sim 2.5$. Lab and field measurements confirm $\beta \sim 2.5$ for small-scale ejecta (Melosh 1989). In any distribution with $\beta < 3$, mass is concentrated at the high-d end. However, the distribution truncates at some high size, which depends mainly on the abundance of mechanical defects in the target. A planetesimal or asteroid probably has mechanical defect abundance at least comparable to that of the deep lunar crust (Nolan et al. 2001). Based on observations of the rims of lunar craters and of blocks on Ida, Lee et al. (1996) postulated a simple relationship between the largest ejecta block size L ("size" here is the observable maximum dimension, which is probably a little larger than an equivalent diameter) and the crater diameter (final D, not D_t) for craters in these targets: $L \sim 0.25D^{0.7}$. Based on this model, comparison with the total ejecta volume (1c) indicates that the craters of interest here yield largest fragments that have masses amounting to approximately 0.0003 (D of order 500 km) to 0.02 (D of order 5 km) percent of the total ejecta mass. Assuming $\beta \sim 2.5$ for all smaller fragments, only half of the total ejecta mass would be in fragments $< 0.044\times$ as massive as the largest; only 25% would be in fragments $< 0.0036\times$ as massive as the largest. Taken at face value, this model implies that survival of large blocks is a more important issue for smaller bodies. However, there may be an offsetting tendency for material toughness, i.e., large-fragment survivability, to decrease with decreasing d_B.

Cintala and McBride (1995) found evidence in that in general the largest blocks ejected from lunar craters are not as numerous as implied by simple power-law extrapolation from the size–frequency distribution among smaller surface debris (cf. fragmented geological materials in general, e.g., Blenkinsop 1991; Barnett 2004). However, the vestoid asteroids, which probably represent ejecta blocks from Vesta's 460 km southern hemisphere basin (Asphaug 1997), are larger in d (up to 14 km; Kelley et al. 2003) by a factor of 6 than predicted by Lee et al.'s (1996) model. The timing of the biggest crater's origin may be important for the large ejecta issue. If the largest crater forms early, then its biggest ejecta will be prone to demolition by subsequent cratering. If the largest crater forms after a history of bombardment by comparably big impactors, then the battered target interior will be more prone to break into small bits; *unless* in the mean time the interior has undergone heating to igneous or near-igneous temperatures. In the igneous scenario, unless a very large impact occurs while the body is unusually susceptible to disruption (see, e.g., Warren and Huber 2006), its interior, left undisturbed, will eventually reconsolidate into strong solids. Vesta may be an example of this scenario.

The Regolith Within the Megaregolith

Regolith sensu stricto (especially fine-grained and porous surficial ejecta-debris) accumulates locally in area and time whenever small-D/d_B cratering (especially high-b cratering) persists through a stochastic lull in resurfacing events; i.e., high-D/d_B cratering and/or shallow magmatism. As noted by Robinson et al. (2002), the terminology of "megaregolith" versus "regolith" can be confusing. By historical accident, the seminal Shoemaker et al. (1969) work on extraterrestrial ejecta accumulations focused on the unusual context of mare lava plains, where the powdery lunar surface regolith is separated by only a few meters from near-intact bedrock (mare basalt, emplaced too recently to be thoroughly disaggregated). However, heavily cratered terrains such as the lunar highlands, where the regolith is underlain by megaregolith (the term was coined by Hartmann 1973), do not fit as well into the original scheme of powdery regolith abruptly giving way to coherent bedrock. Asteroid geologists commonly draw little distinction between megaregolith and regolith, applying the latter term to any and all accumulated ejecta-debris (e.g., Housen et al. 1979). Nolan et al. (2001) extended megaregolith to include deep interior material that is impact-fragmented into coarse "rubble" without ever being ejected from a crater. As noted above, I prefer a definition that limits megaregolith to accumulated ejecta. In the lunar context, compared to megaregolith, regolith is distinctively finer in median grain size, much more porous, and richer in materials whose origins require exposure at the very surface, such as small impact-melt spheroids, implanted solar-wind noble gases, and agglutinates (Wilhelms 1987; Warren 2001a).

In terms of thermal implications, a regolith within a megaregolith is analogous to the megaregolith within the 8 km thermal "skin" modeled with Fig. 2 and Equation 1. Results (again assuming a steady state, neglecting internal heat generation; admittedly over-simplistic) for the relative q implied by various assumptions regarding the regolith and megaregolith thickness and conductivity are shown in Fig. 15. For a regolith having approximately 0.1 times the megaregolith conductivity k_{MR} (cf. Fig. 1; the 1 m deep

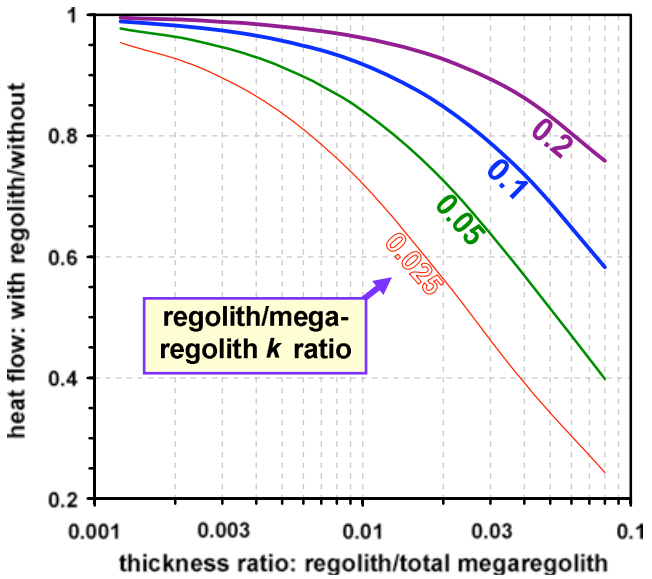

Fig. 15. Relative heat flow q as a function of the regolith/(total megaregolith) thickness ratio, shown for a range of assumed relative conductivity k of the regolith and megaregolith. These results are applicable to bodies of all sizes, and a wide range (0.001–0.01) of assumed megaregolith thickness/r_B ratio (varying megaregolith thickness/r_B within this range has negligible effect on the relative q).

soils probably have slightly lower k than the overall several meters thick regolith), the regolith thickness must reach 11% of the overall megaregolith to cause a 50% increase in its overall thermal resistance. For comparison, the thickness of the lunar megaregolith is suspected to be approximately 2–3 km (Warren and Rasmussen 1987); and the top approximately 0.5–1% of that thickness (in the maria, ~0.2%) is regolith sensu stricto (Wilhelms 1987). Figure 15 thus suggests that the Moon's rather thin regolith reduces heat flow through the overall megaregolith by a mild factor of approximately 0.9.

As discussed above, maximum crater excavation depth ω_{max} is never much greater than $0.1D_t$, so anywhere that a surface is exposed to a bombardment of tens-of-meters-scale and smaller cratering with a high b (at these scales, from a variety of evidence, $b \sim 3.5$; Melosh 1989) the upper few meters will grow increasingly pulverized, until some event resurfaces the area with rocky matter. Aspects of the impact process also "erode" regolith (Housen et al. 1979), but unless an impact is very large, while the global regolith is modified in detailed shape, its total volume is little changed. On the Moon's maria-rich near side, the last resurfacing event was commonly basaltic lava extrusion. But more generally the resurfacing mechanism will be a mass of ejecta (new megaregolith) from one of what Housen et al. (1979) termed "scattered, large anomalous craters." On a large body such as the Moon, the simple mass-addition effect is greatly enhanced by the jumbling that occurs ("ballistic sedimentation"; Oberbeck 1975) when large distal ejecta land at velocities that are major fractions of the body's escape velocity (2.4 km s^{-1}, for the Moon). Haskin et al. (2003) estimate that a single $D_t/d_B \approx 0.21$ event, Imbrium, by a combination of churning and (at proximal locations) simple deposition, thoroughly reconstituted the megaregolith at practically all locations around the globe to a depth of at least 500 m. In detail, this estimate is sensitive to the size distribution and launch angle assumed for the distal ejecta, and to the strength-resistance of the megaregolith against secondary churning. But it seems clear that virtually no lunar regolith, sensu stricto, survived through this one 3.9 Ma (Wilhelms 1987) event, except in the form of regolithic clasts within the megaregolith. Thus, it is naïve to assume (e.g., Wilson et al. 2008, p. 6158) that some fraction of the present few tens of meters of lunar highlands regolith is all that ever formed during the first 1/2 Ga on this body.

A volume of regolith that becomes thoroughly dispersed as a minor component within a jumble of megaregolith will marginally increase the porosity and thermal insulation of the megaregolith, but its effect on overall heat loss is not nearly as great as the effect when the regolith remains in place as a laterally continuous thermal barrier. Haskin et al.'s (2003) model (cf. Petro and Pieters 2008) implies that events with D_t/d_B as small as approximately 0.13 are probably big enough to recycle effectively (i.e., churn-dilute by a factor of at least 5, which would leave the porosity, for example, only a few percent higher than the approximately 17% characteristic of the overall megaregolith) all regolith within 30 m of the surface on one hemisphere of the Moon; and a combination of three to four such events, at random locations, would suffice to destroy virtually all regolith. Events of this D_t/d_B are probably common during the overall accumulation of a megaregolith. For example, if $b = 2$ and $D_L/d_B = 0.5$, with average sampling there will be a total of 16 craters with $D_t \geq 0.125 d_B$.

On smaller (d_B not $>> 100$ km) bodies, the churning when distal ejecta land is probably less effective. Secondaries land at velocities never higher than v_{esc}, which for uniform density is directly proportional to d_B. However, if small-body megaregoliths are weakly cohesive, as might be expected from, inter alia, the expected lesser proportion of melt in small-body impacts (Melosh 1989), that lack of cohesion might largely offset the difference in landing velocity. Also, the small-body enhanced process of launch-off will from time to time cause regional regolith destruction (cf. Housen et al. 1979).

If this analysis is correct, the lunar-science custom of distinguishing between megaregolith and regolith also has merit for asteroids and planetesimals, at least for those $>>100$ km in d_B. The destruction of regolith in rare but almost inevitable large events means that the distribution of material types truly is to a considerable degree bimodal. Meteorite samples are of little help in constraining this issue, because as lunar samples show (Warren 2001a), only regolith breccias that are extraordinarily tough will commonly survive the rigors of transit down to Earth's surface. In any event, in terms of global thermal insulation, the regolith (sensu stricto) is unlikely to ever become thick enough to be important compared with the megaregolith.

Porosity Reduction: I. Simple Compaction and Aqueous Metamorphism

The porosity engendered by accumulation of ejecta into a megaregolith is incremental to whatever residual accretionary porosity the body retains in its deeper interior. Realistically, most planetesimals consist mainly of fractured rock, with at least slight porosity, from their very beginnings. Planetesimal growth occurs through impact-agglomeration of countless former target bodies. The net effect of each impact is usually an increase in the overall fracturing and porosity of the target, albeit impact-compaction is locally effective with already porous targets (Housen and Holsapple 2003; Scott and Wilson 2005) during relatively gentle impacts, which were common during early stages of accretion (Weidenschilling and Cuzzi 2006), or through impact melting during end-stage impacts between megameter-scale bodies. Wilson et al. (1999) modeled in a qualitative way the evolution of porosity during generations of successively disrupted and reassembled planetesimals, and suggested that 20–40% was probably the typical outcome. Nolan et al. (2001), among many others, have also discussed the development of deep porosity in small bodies by nonejective impact processes.

Housen and Wilkening (1982) referred to such material as "accretionary megaregolith," but envisaged that it tended to be "destroyed by being converted into cohesive material by heating or gravitational compaction." Sintering will be discussed below. Near-surface, low-T compaction probably was roughly comparable in effectiveness on smaller bodies as within the Moon. In its upper few meters, the lunar regolith is far less porous than would be expected on the basis of simple self-weight compaction (Stesky 1978). Carrier et al. (1991) suggested that impact-seismic shaking contributes to this enhanced compaction. Impact-seismic shaking is now appreciated as an important surface modification process on asteroids (e.g., Asphaug 2008). Compaction must also, locally, be enhanced by impact-induced compression, including the gentle impacts of large secondaries, especially if the preimpact porosity is very high (Housen and Holsapple 2003).

As estimated by Carrier et al. (1991; their fig. 9.16), the lunar regolith compacts from approximately 60% porosity at the very surface, to approximately 43% at depth of 1 m, where P is still just 0.0029 MPa; to approximately 36% at 10 m where P is 0.029 MPa (assuming regolith $\rho \approx 1800$ kg m^{-3}). For $\phi = 36\%$, the lunar porosity–conductivity relationship (Fig. 1) implies $k \sim 0.02$ W m^{-1} K^{-1}, i.e., about one-tenth of the lunar megaregolith's k. For comparison, assuming a shallow-interior density of 2000 kg m^{-3}, the pressure P_{95} at which 95 vol% of the body is deeper (i.e., at $r/r_B = 0.95^{1/3}$) is approximately $5 \times 10^{-12} d_B^2$ (for d_B in m and P_{95} in MPa); and thus the d_B of a body with $P_{95} \sim 0.029$ MPa is 79 km. A 200 km (d_B) body has a P_{95} approximately 6.5 times the P at which compaction within the lunar regolith modifies porosity to approximately 36%, and k to approximately 0.02 W m^{-1} K^{-1}. This analogy between the Moon and much smaller bodies should not be overdrawn. Many asteroids have bulk densities suggestive of $>36\%$ porosity (Britt et al. 2002), and regoliths on smaller bodies may differ in material properties (most importantly grain size) from the lunar archetype (Asphaug 2009). Intragrain porosity, insusceptible to reduction by low-P compaction, may greatly augment the intergranular porosity that is susceptible. But the lunar analogy does suggest (1) that real-world vacuous planetary compaction, even at low, fixed T, is more complex and efficient than simple self-weight static compression; and (2) that planetesimal models (Hevey and Sanders 2006; Sahijpal et al. 2007) assuming presintering $k \sim 0.001$–0.002 W m^{-1} K^{-1}, corresponding to approximately 60% porosity, may not be entirely realistic.

On warm and water-rich planetesimals, porosity might be further reduced by the formation of chemical precipitates, such as carbonates, sulfates, halides, and oxyhydroxides, as well as hydrous silicates, such as serpentines and clay minerals, through aqueous metamorphism (Grimm and McSween 1989; Brearley 2006). Liquid water is potentially abundant for temperatures from 273 K to its critical point at 647 K and 22 MPa; and its vaporization T is roughly $500 + 80 \log P$ (for P in MPa). If liquid water is abundant and the body is sufficiently large (high-g) and permeable, hydrothermal convection will occur (Young et al. 2003); in which case convective energy transport will greatly augment conductive heat flow, and thereby hold temperatures, at least in the shallow interior, close

to the P-governed H_2O vaporization T. If the body is permeable but too small to sustain hydrothermal convection (this condition would hold up to $d_B \sim 120$ km: Young et al. 2003), water mobilized by warm-up will simply flow in a "single pass" up toward the shallow interior. The water tends to become concentrated in the shallow interior, most obviously in the single-pass scenario, but probably also eventually in the case of hydrothermal convection (which as it wanes must come to resemble single-pass flow), particularly if the body's deeper interior undergoes continued warming into the temperature range of dehydration (~700–800 K, e.g., Grimm and McSween 1989) and/or sintering-densification (see below). If the water collects mostly in the shallow interior, eventually most of the final products of aqueous metamorphism will also be concentrated there.

The mineralogical changes associated with aqueous metamorphism would diminish porosity, both by directly filling pores (with chemical precipitates such as carbonates) and by replacing dense anhydrous mafic silicates with low-density hydrous derivatives. The reduction in porosity will be particularly drastic if the new hydrous silicates include expansive clays such as saponite, which is abundant in some carbonaceous chondrites (Zolensky 1995). However, water mobilized near the surface of a small body is also prone to be lost by venting, evaporation, and (after crystallization near the cold surface) sublimation, particularly if the shallow interior is both warmed and fractured by intensive impact gardening. A scenario of major aqueous-metamorphic densification probably requires not only that the body's initial bulk composition be water-rich, but also that its surface happens to avoid large-D/d_B cratering during the stage of aqueous flow.

Porosity Reduction: II. Sintering

Sintering can destroy megaregolith from the bottom up, by a form of global thermal-burial metamorphism. As noted by Sahijpal et al. (2007), sintering may also work from the top down, in the event of massive extrusions of lava. However, to invoke that scenario is to obviate the main concern with megaregolith, i.e., whether the body can retain heat efficiently enough to become anatectic. Hevey and Sanders (2006) assumed that sintering occurs in a warming planetesimal as the temperature passes 700 K, and changes the material from lunar regolith-like in terms of porosity into solid rock, thus causing a sudden increase in k by almost three orders of magnitude. Sahijpal et al. (2007) likewise assumed that sintering, and a factor of 1800 increase in k, occurs at 670–700 K. But these were mere assumptions, citing Yomogida and Matsui (1984) for derivation of the sintering temperature. Akridge et al. (1998) assumed that in small bodies sintering is negligible, and thus k remains similar to that of lunar regolith, even at $T \sim 1200$ K.

Densification, the gradual elimination of porosity by sintering, is a complex function of temperature, time, pressure, and material properties (German 1996; Kang 2005). Materials-scientists recognize three distinct stages of sintering-densification. The initial stage involves growth of "necks" between loosely packed grains with minimal grain coarsening. The second stage involves moderate grain coarsening and, eventually, elimination of interconnective porosity. The third stage sees major coarsening and, usually, slight further densification. At temperatures less than about two-thirds of the melting T, each stage is of long duration. If near the second–third stage transition grain coarsening happens too fast relative to pore-size reduction, "breakaway" of pores from grain boundaries can effectively forestall the elimination of the final ~10% of porosity, so that full densification may require "precise manipulation of the initial powder microstructure and heating cycle" (German 1996).

Poppe (2003) conducted a series of experiments for constraining the sintering behavior of extremely porous (95%) amorphous SiO_2 spherules 0.78 μm in r. He extrapolated his results to estimate that 0.1 MPa sintering of this material takes approximately 1 Ma at 1000 K. It may be unwise to even attempt extrapolation from these results to the sizes, intragrain porosities, compositions, and pressures relevant to this work.

Yomogida and Matsui (1984) inferred "600–650 K" as the most likely temperature "where sintering starts to become important." However, this estimate was based on a single assumed lithostatic pressure P (~1 MPa), albeit they explicitly modeled the sintered k as sensitive to an "effective stress" of 10 MPa (more will be said about "effective stress" below). Even the deepest level to which ejecta accumulation extends (Fig. 12) will not have P as high as 1 MPa unless the body is bigger than roughly 200 km in diameter (Fig. 3; lithostatic P scales as d_B^2). Also, more recent measurements have shown that the rate of deformation of olivine is sensitive to the presence or absence of water, and the grain-boundary diffusion data used by Yomogida and Matsui (1984; from Schwenn and Goetze 1978) appear suitable for "wet" olivine but fast relative to "dry" olivine, by roughly an order of magnitude in "effective diffusion constant" (Karato et al. 1986). As one gauge of the potential importance of water, Faul and Jackson (2007) note that the time needed for 1200 °C growth to 1 mm grain size in olivine aggregates may vary from approximately 1 yr in wet conditions to tens of Ma in otherwise equivalent dry conditions.

Although most megaregolith matter is probably crystalline, not glassy, sintering can be most readily constrained for glasses, where its rate and duration t_S are determined by viscous flow. It seems unlikely that crystalline mafic silicates would sinter-densify faster than mafic silicate glass, so the glass rate may be viewed as an upper limit on the rate for crystalline matter. Simonds (1973) applied a viscous-flow model to the sintering of lunar-basaltic glass. Assuming spheroidal grains, the governing equation (cf. German 1996) is

$$t_s = \left(\frac{2}{3}\right)(\eta/\gamma)(X^2/r), \tag{8}$$

where η is the T-dependent viscosity, γ is the surface-interfacial energy (surface tension), r is the grain radius, and X is the assumed radius of the neck between touching grains. For modeling t_S at the late-initial stage of sintering, I assume $X = r/5$ (Simonds 1973) and $\gamma = 0.5\ \mathrm{J\ m^{-2}}$ (Cooper and Kohlstedt 1982). To represent the T-dependent η, I employ the results of Cukierman et al. (1973) for the composition of lunar olivine basalt 15555 (similar η is implied by a wide variety of basaltic compositions; the viscosity data set used by Simonds was never explicitly published). With these parameters, Equation 8 indicates that the T for the late-initial stage of sintering, assuming a grain radius of order 0.1 mm and a t_S of order 1–5 Ma, is approximately 785 K ($\pm$15 K for any factor of 10 variation in the grain size; given the likely crucial importance of ^{26}Al in primordial heating, the duration of sintering in all but the largest of planetesimals was probably limited to $<<$10 Ma). Zagar (1979) extended this model into one that explicitly addresses the diminution of porosity ϕ. In German's (1996) slightly simplified form, Zagar's equation is

$$t_s = -2r\,(\eta/\gamma)\ln(\phi/\phi_i), \tag{9}$$

where ϕ_i is the initial, presintering porosity. Results, based on the same parameter assumptions as used for Equation 8, are shown for a range of porosity reduction factor and r in Fig. 16. Assuming r of order 0.1 mm, Fig. 16 implies that basaltic glass would have gone through the intermediate stage of sintering at approximately 820 K. But this merely represents a 0.1 MPa result. The process would go faster (or in a given time period, at lower T) at the P of the base of a megaregolith on a large asteroid or planetesimal (Fig. 3), and faster still in a large body's deep interior. Still, it is noteworthy that at low P, sintering of basaltic glass occurs at a considerably higher T than Yomogida and Matsui (1984) estimated for sintering in general.

During pressure-sintering, ambient pressure is amplified into an "effective stress" or pressure P_E that develops at contact areas between grains. If P is high enough to be a controlling factor (German 1996 indicates this condition begins at a P of order 0.1 MPa), the time t_S for a given extent of sintering-densification scales as P_E^{-1} (Kang 2005, equation 5.23). German's (1996) equation 7.8 indicates that P_E may be approximated well enough for present purposes (assuming vapor pressure even in closed-off pores remains low) as a function of porosity:

$$P_E \sim P e^{(6.7\phi)}. \tag{10}$$

This approximation is valid for the ϕ range 0–1/3. If ϕ exceeds 1/3, the approximation begins to significantly underestimate P_E/P. As some examples, as ϕ approaches zero, the P_E/P ratio approaches 1, but $\phi = 25\%$ implies $P_E/P = 5$; and $\phi = 33\%$ implies $P_E/P = 13$. In short, for the ϕ range (say 10–25%) relevant to the early stages of megaregolith sintering P_E/P is roughly 3, but for reduction of the first half of the porosity from a powdery (Moon-style) regolith P_E/P is $>>10$.

Summing up, "the" temperature of sintering-densification T_S is a function of, inter alia, both pressure and the order of magnitude abundance of water, which by speeding diffusion enhances sintering. If T_S is considered to represent a reduction in porosity to final value of order 10%, then estimating $dT_S/d(\log t_S)$ to be 146 $\pm$ 34 K (Akechi and Hara 1979; Alister et al. 1979; German 1996; Kang 2005) and assuming grain size (r) of order 0.1 mm, as a rough approximation we arrive at

$$T_S \sim A - 146\log_{10}(10P_E) \tag{11}$$

where T_S is in K, P_E is in MPa, and A ranges from approximately 900 K for water-rich conditions (which makes for agreement with Yomogida and Matsui 1984 who assumed $P_E = 10$ MPa) to roughly 1300 K (constrained mainly by tenuous extrapolation from the grain-growth observations of Faul and Jackson 2007) for anhydrous conditions. Equation 11 is only valid for $P_E > 0.1$ MPa; at lower P, $T_S \sim A$.

The abundance of water is difficult to constrain. Most igneous meteorites, representing several tens of separate parent bodies (many different types of irons; several varieties of primitive achondrites; ureilites; aubrites; and howardites, eucrites, and diogenites, including some anomalous eucrites [Nyquist et al. 2009]), contain Fe-metal, which is an almost certain indication of anhydrous origin. Water is prone to react with Fe-metal to form FeO (+ultra-fugacious H_2; McSween and Labotka 1993). Even in these cases, however, water may have been significant at some stage of the parent body's warm-up.

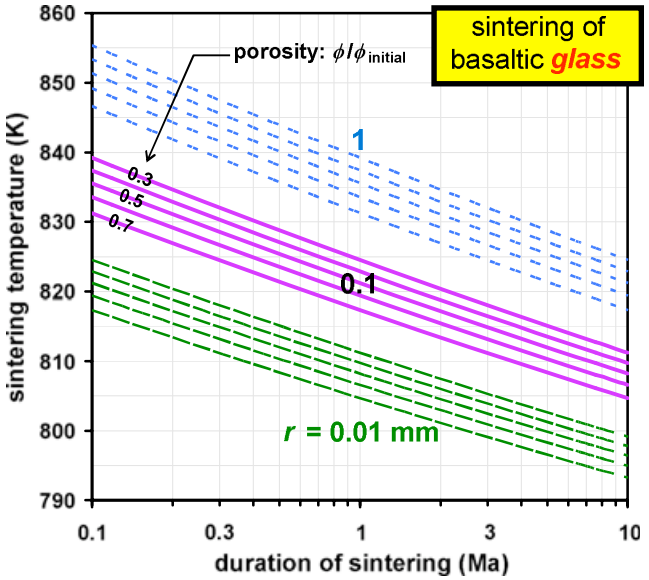

Fig. 16. Time–temperature relationships for intermediate-stage sintering of spheroids of basaltic glass, modeled as an isothermal process by the method of Zagar (1979) for grain size (r) of 0.01–1 mm and porosity/initial porosity ratio (ϕ/ϕ_i) of 0.3–0.7.

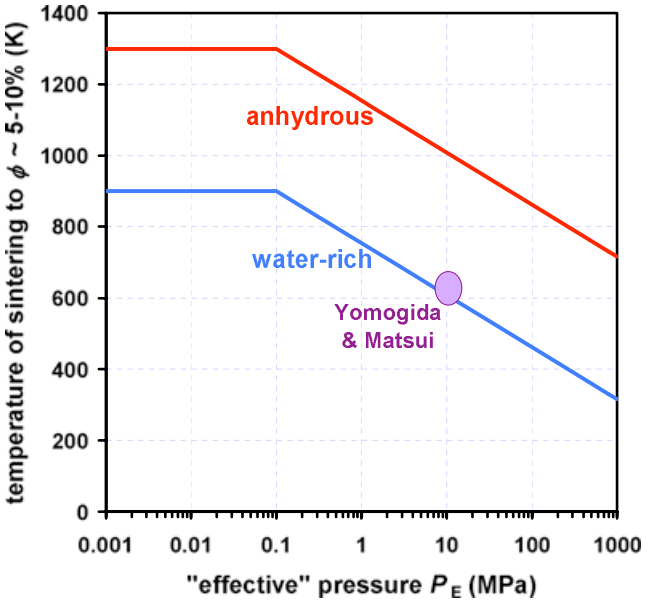

Fig. 17. Sintering temperature T_S, for reduction of porosity to roughly 5–10%, calculated as a function of "effective" (grain-contact) pressure P_E using Equation 11.

The sintering temperature T_S implied by (11) is shown in Fig. 17; and also, with P_E translated into combinations of d_B and depth, in Fig. 18 (for two values of porosity, 5–15%). The reduction in porosity from 15% to 5% has about the same effect on T_S as decreasing depth within any given body (i.e., lithostatic pressure) by a factor of 2.

Near the surface, assuming equivalent density, the pressure–depth gradient dP/dz (Fig. 3) is directly proportional to d_B. Pressure within the ejecta accumulation zone will range from zero at the surface to $P(z_A)$ at the zone's basal depth. If m_L tends to be in some consistent proportion to the critical impactor mass m_C, so that the final ejecta accumulation thickness (in kilometers) scales roughly as d_B (Fig. 12), then $P(z_A)$ and the other pressures within the zone, e.g., $P(0.5z_A)$, will be proportional to d_B^2. Thus, as the bodies heat, sintering will densify the lower ejecta accumulation zone at a much lower T_S in a big body than in a small one (Fig. 19). Except for the uppermost approximately 10% of the ejecta accumulation zone (and only then in large bodies), the range in T_S within any given ejecta accumulation zone is mild in comparison to the T_S diversity that arises as a function of d_B. Figure 19 shows results for only one assumed m_L/m_C, but the effect of a different m_L/m_C is also comparatively mild; e.g., the T_S of the bottom of the zone varies by approximately 50 K as the assumed m_L/m_C ratio is varied (for any given d_B) from 0.25 to 0.75.

The sensitivity of T_S to d_B means that destruction of megaregolith by sintering is more efficient on larger bodies. As heating proceeds, smaller bodies end up maintaining almost full insulation from their comparatively thin ejecta accumulations at temperatures where on larger bodies the megaregolith's thermal resistance is reduced by a large factor. For example, at 1100 K, ejecta-zone sintering is still, according to (11), negligible for porosity up to approximately 16% on a body 150 km in d_B, in which the bottom of the ejecta zone, for $m_L/m_C = 0.5$ (as assumed for Fig. 19) is approximately 4.6 km deep. By contrast, in a 1000 km (d_B) body at 1100 K, sintering will have densified to $< 5\%$ porosity (i.e., k within a factor of two of solid rock) everything deeper than approximately 1.3 km. The same relationships would apply at approximately 700 K in a water-rich body.

Even a few hundred meters of megaregolith will constitute a significant thermal resistance. The thermal evolution will be determined by a complex interaction (beyond the scope of this work) between heat generation and heat loss, as moderated by the megaregolith's insulation. But these considerations indicate that for the crucial transition from a hot but still solid interior, to an interior that undergoes (beginning at roughly 1400 K) extensive melting, size of the body is not so all-important as it would be in the absence of megaregolith insulation. The metamorphic versus igneous-differentiation fate of a body may depend almost as much on the stochastic (although

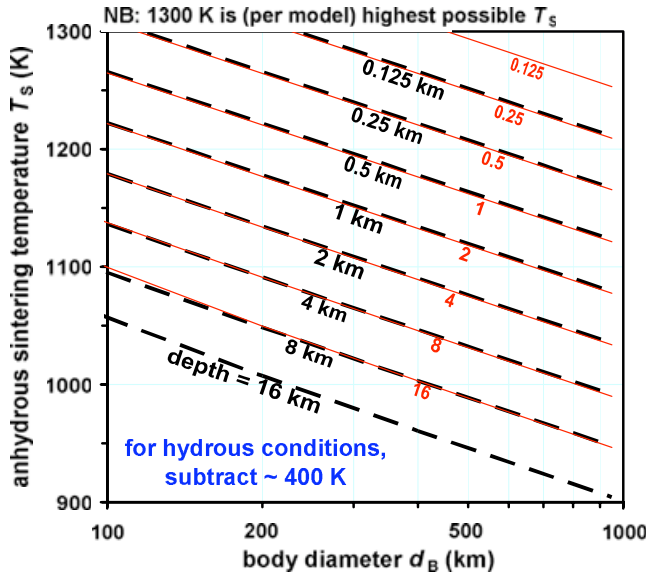

Fig. 18. Sintering temperature T_S, calculated as a function of target-body diameter d_B and depth (i.e., P). Results are calculated for sintering through two porosities: 15% (heavy dashed curves) and 5% (light continuous [red] curves).

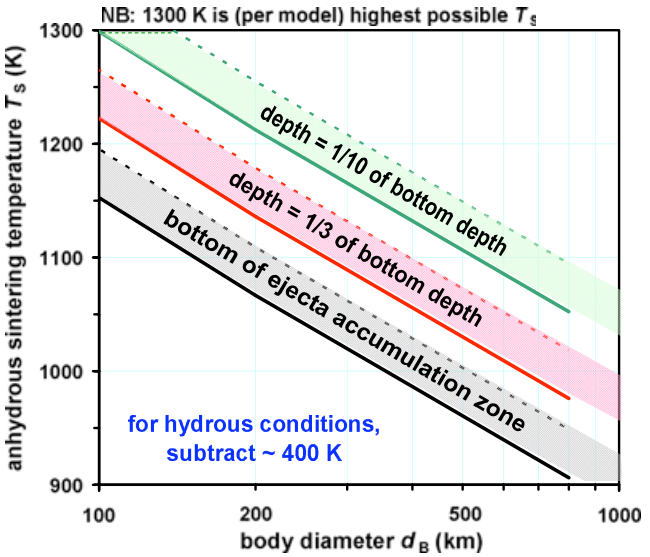

Fig. 19. Sintering temperature T_S, calculated as a function of target-body diameter d_B assuming that the largest crater is formed with $m_L/m_C = 0.5$; i.e., the impactor mass m_L is 50% as massive as the catastrophic-disruption mass m_C, as calculated by extension of the model of Bottke et al. (2005a, 2005b). Results are calculated for three levels within the ejecta accumulation zone (whose bottom depth is z_A), and for sintering through two porosities: 15% (heavy-continuous curves) and 5% (light-dashed curves).

undoubtedly d_B-correlated) m_L/m_C result, which determines its ejecta accumulation z_A, as on its sheer size and initial heat-source (^{26}Al) content.

Comparison with Past Work, Known Asteroids, and the Moon

As reviewed by Housen and Wilkening (1982), early work on the issue of asteroidal regolith development typically assumed that most ejecta undergo launch-off during impacts onto hard, solid-rock surfaces, leaving only thin accumulations except on the largest asteroids. In their time-keyed modeling, Housen et al. (1979) still predicted that only a thin ejecta accumulation (“regolith,” in their simple terminology) develops on most asteroids; e.g., over 10^9–10^{10} yr “a few hundred meters” thickness develops on a 100 km (d_B) asteroid, and 0.9 km on a 300 km asteroid. Those results are lower by a factor of approximately 10 than results derived here for $m_L/m_C \sim 0.5$ (Fig. 12; Table 1). The main reason for this discrepancy is that Housen et al. assumed much smaller m_C and D_C (m_r and D_r in their terminology), and thus much smaller D_L. My results show agreement with Housen et al. (1979) if I assume D_L/d_B is fixed at approximately 0.5.

Housen et al. (1999) and Housen and Holsapple (2003) revisited impact cratering on porous asteroids, but their studies were focused on extremely porous (34–96%) targets (cf. Benz and Jutzi 2007; Ciesla et al. 2009). As discussed above, analogy with the lunar regolith suggests that porosity $>>40\%$ is probably seldom sustainable on even a cold body $>>50$ km in diameter, except very near the surface where $P < 0.003$ MPa (cf. Fig. 3; as mentioned in the figure’s caption, adjustment for bulk density is required). In any event, to assume such high target porosity in the largest events obviates the question of whether or not the megaregolith becomes thick enough to have important thermal consequences.

Ward (2002) also gave estimates for the ejecta accumulation thickness for three different assumed target-body sizes; and from those, it is possible to interpolate to various other sizes (Table 1). Like Housen et al. (1979), Ward chose to estimate cratering effects as a function of an assumed duration and rate. My choice, for the comparison in Table 1, of 5 Ga and a rate of 10 times the present-day (Earth) value is arbitrary. Ward’s modeling did not consider effects of different target-body size, such as the role of g in determining the d_i/D_t ratio.

Figure 10 shows the largest observable crater diameters D_{LO}/d_B for several large rocky asteroids (Asphaug 2008) and the Moon. These D_{LO}/d_B are lower by factors of approximately 2–3 than the D_L/d_B ($\sim$1) suggested by modeling the largest impactor mass as

Table 1. Global ejecta accumulation results (z_A, in km) compared with previous work.

d_B (km)	100	200	300	800	Duration
Housen et al. (1979)	~ 0.3	–	0.9	–	10^9–10^{10} yr
Ward (2002)*	2.1*	2.5*	2.7*	3.3*	5 Ga
This work, $b \equiv 2$, $D_L/d_B = 0.5$	0.36	0.7	1.1	2.8	N/A
This work, $b \equiv 2$, $m_L/m_C = 0.5$	4.1	6	8	18	N/A
$b \equiv 2$, $m_L/m_C = 0.25$	1.8	3.6	5	11	N/A
{variable b}, $m_L/m_C = 0.5$	{2.3 → } 4.4	{1.4 → } 4.8	{1.6 → } 6.5	{3.0 → } 27	N/A
{variable b}, $m_L/m_C = 0.25$	{2.3 → } 2.0	{1.4 → } 2.7	{1.6 → } 4.2	{3.0 → } 18	N/A

Note: Ratio m_L/m_C is probably anomalously high at $d_B \sim 100$ km (see text). The choices for variable b, shown in {brackets}, conservatively equate the β implied in Fig. 7 with b.
*For Ward (2002) results, I have very arbitrarily selected 10× present-day cratering rate; the present-day rate would imply accumulation thicknesses approximately 0.14× those shown.

roughly 0.5 times the catastrophic-disruption mass m_C (Fig. 7). However, these observations are best viewed as lower limits on the largest impacts experienced by these bodies. Impact-seismic shaking is effective at smoothing over the surfaces of smaller bodies, and Asphaug (2008; however, cf. Richardson et al. 2005) has inferred that this seismic process, rather than survival against impacts with mass ~ m_C, limits the observed asteroidal D_{LO}/d_B ratios; and the size dependency of the process leads to the decrease in D_{LO}/d_B with decreasing d_B. Vesta and especially the Moon were hot enough for long enough that all manifestations of their largest impacts have quite possibly been erased by internal dynamism.

Asteroids have by definition experienced a longer, colder evolution than typical planetesimals. After asteroids cooled to the point where sintering became insignificant, they continued to undergo a long history of reduced-intensity but nonetheless cumulatively important impact cratering. Thus, overall porosity is expected to be generally much higher within a large asteroid than in a typical similar-sized warm planetesimal. As reviewed by Britt et al. (2002), asteroid porosities, inferred for approximately 20 bodies (including Phobos and Deimos) from observed density and estimated "grain" density, are diverse but generally high. Even for the 15 largest ($d_B > 50$ km) bodies, average porosity is 35%. Only the three most massive asteroids show clear evidence of size-related diminution of porosity (Pallas, Vesta, and Ceres, average $\phi = 5\%$). Asteroids as massive as 2×10^{19} kg ($d_B \sim 270$ km) show no such evidence. Unfortunately, no constraints are available for asteroids with d_B between approximately 270 and 520 km.

Asteroids much smaller than 50 km (d_B) are outside the scope of this work, and undergo a different style of cratering (strength regime) that in combination with their low escape velocity is unfavorable to retention of ejecta. Observations suggest that their (mega)regoliths are indeed thin (Chapman et al. 2002; Robinson et al. 2002; Sullivan et al. 2002), albeit ejecta retention is far more efficient than most pre-1991 (*Galileo*'s visit to Gaspra) models predicted. The largest constrained asteroids are Mathilde (equivalent $d_B \sim 53$ km), and to some extent Vesta. Mathilde has a whole-body porosity of approximately 52% (Britt et al. 2002), making demarcation of a megaregolith within its shallow exterior impossible, given the limited observational evidence. The *Dawn* mission (Russell et al. 2004) will soon reveal much about Vesta. As discussed above, Vesta appears to have undergone an unusual evolution. After extensive melting, much of its interior was annealed, which probably imparted an extreme "monolithic" strength. Much later, its present megaregolith was produced (along with the vestoids) largely through the formation of one exceptionally large and late crater. For both Vesta and especially the Moon, the present megaregolith thickness probably reflects only a fraction of the total cratering, as the earliest surfaces were overprinted by magmatism. For the Moon, based on seismic and crater-morphologic data (Head 1976), the geometries of large lunar grabens (Golombek 1979), and radar data indicating that as lunar craters exceed approximately 20 km in diameter D they begin to excavate a more cohesive type of material (Thompson et al. 1979), the megaregolith thickness appears to be roughly 1.5–3 km, increasing (possibly to much more than 3 km) with proximity to the South Pole-Aitken basin (Thompson et al. 2009). Within uncertainty, this agrees with modeling (Fig. 10) if South Pole-Aitken is the largest impact since crustal genesis and sintering has not destroyed (densified) a large fraction of the total ejecta accumulation. Sintering might yield a notably gradational megaregolith/solid crust transition, but the available constraints on the transition are far from conclusive in this respect.

The Thermal "Skin" Issue, Revisited

As discussed in the Introduction, a planetesimal that undergoes rapid heating by a uniform-distribution heat

source (such as, before differentiation ^{26}Al) will tend to evolve into an approximately isothermal interior beneath a thermally graded "skin." Turcotte and Schubert (1982) showed with their equation 4–115 that for the simple case of cooling with negligible heat production, the thickness of the thermal boundary layer z_{skin} is given by

$$Z_{skin} = 2\eta(\kappa t)^{1/2}, \quad (12)$$

where κ is the thermal diffusivity (i.e., $\kappa = k/(C_P\rho)$ where C_P is the specific heat capacity and ρ is the density); η is the inverse complementary error function of θ (i.e., $\mathrm{erfc}(\eta) = \theta$); and θ is the ratio $(T_{base} - T_{surface})/(T_{deep} - T_{surface})$, where "base" refers to the base of the skin layer.

For the more relevant scenario of a spherical body with internal radioactivity generating heat at the rate $A_0 e^{-\lambda t}$, a solution for the temperature profile was derived by Carslaw and Jaeger (1959; equation 14 on their page 245):

$$T = \frac{\kappa A_0}{k\lambda} e^{-\lambda t}\left(\frac{a \sin r[\lambda/\kappa]^{1/2}}{r \sin a[\lambda/\kappa]^{1/2}} - 1\right) + \frac{2a^3 A_0}{r\pi^3 k}\sum_{n=1}^{\infty}\frac{(-1)^n}{n(n^2 - \lambda a^2/\kappa\pi^2)}\sin\frac{n\pi r}{a} e^{-\kappa n^2\pi^2 t/a^2}, \quad (13)$$

where A_0 is the initial rate of heat production, λ is the decay constant, a is the body radius, and r is the position under evaluation expressed as a fractional radius. As long as the heat-loss mechanism does not change (e.g., by high T triggering convection), neither the choice of A_0 nor the size of the body has any significant effect on the relationship between t and z_{skin}. The thickness of the skin layer implied by (13) is shown as a function of t and κ in Fig. 20. Inclusion of heat production leads to a slightly reduced skin thickness in comparison to the z_{skin} of the simple model of cooling without heat production; e.g., at t = 2.84 Ma (four ^{26}Al half-lives) the effect ranges from a factor of 0.82 (θ = 0.75) to 0.87 (θ = 0.96). A figure showing results for models without heat production is included in Supporting Information (along with, for both models, log-log plots that may be more useful as nomograms). For solid silicate rock, $\kappa \sim 8 \times 10^{-7}$ m^2 s^{-1}, but as discussed above k (and thus, to a good approximation, κ) could easily be 10 times lower for porous-rocky megaregolith, or even several hundred times lower for powdery regolith. Figure 20 indicates that if the thermal skin consists of megaregolith, then at the time of peak temperature in a body heated by ^{26}Al (and negligible ^{60}Fe) to incipient melting, i.e., 3–4 Ma after accretion (Akridge et al. 1998; Hevey and Sanders 2006; cf. age

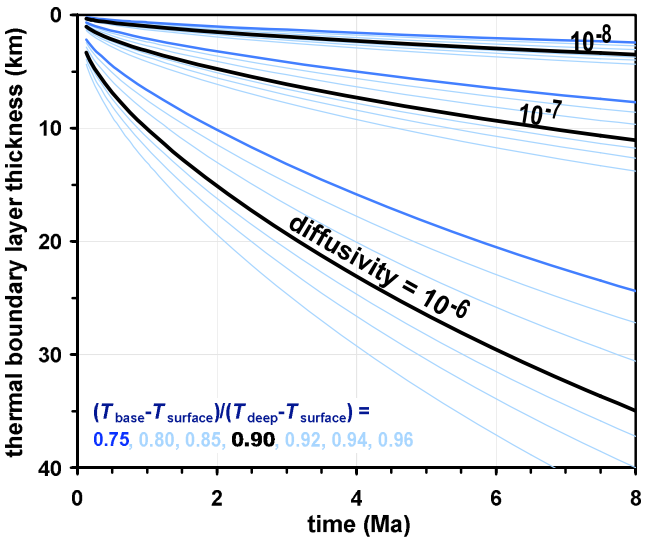

Fig. 20. Thickness of the thermally graded outer "skin" that envelops the approximately isothermal interior of a planetesimal heated by decay of ^{26}Al ($t_{1/2}$ = 0.72 Ma), modeled per Carslaw and Jaeger (1959). Curves are shown for seven different possible values of θ, i.e., $(T_{base} - T_{surface})/(T_{deep} - T_{surface})$; and for three different values of thermal diffusivity κ. To a fair approximation, $\kappa \sim 10^{-6}$ (m^2 s^{-1}) corresponds to a skin that consists of solid rock, 10^{-7} corresponds to a skin of porous-rocky megaregolith, and 10^{-8} to a skin of powdery regolith (sensu stricto). The same diagram is reproduced as a log-log plot (possibly, as a nomogram, more useful) in Supporting Information.

constraints from igneous meteorites: Nyquist et al. 2009), the skin (θ = 0.90) thickness is approximately 7 km.

For much of the range of body size under consideration, the z_{skin} found in Fig. 20 is thicker, even at 2 Ma, than the estimated ejecta accumulation z_A (Fig. 12). As d_B passes approximately 300 km, a m_L/m_C of 0.5 may suffice to make $z_A > z_{skin}$. This comparison assumes uniform k_{MR}. It seems likely that gravity–pressure effects result in a rough anticorrelation between megaregolith porosity and d_B; which would imply a correlation between k_{MR} and d_B, and thus between z_{skin} and d_B. Even so, dz_A/dd_B is probably greater than dz_{skin}/dd_B. In cases where z_{skin} is thinner than z_A, the thermal advantages associated with body largeness will be to some extent moderated.

The limiting factors for planetesimal heat loss will be the lesser of z_{skin} and the megaregolith thickness, along with the k (i.e., the porosity) of the shallow interior above that level. The megaregolith thickness will generally be close to z_A. But it may be significantly less than z_A if the ejecta accumulation has been sintered to an important extent, and/or has not yet grown to its approximate final extent. Even for planetesimals, the

largest crater that ever forms on the body does not necessarily form before the body reaches its peak temperature. For thermal modeling, D_L is the largest crater that (in a statistical sense) has formed as the body has evolved. For that matter, the body's size will not be static as it evolves. However, so long as accretion is oligarchical, the general expectation is that at any given stage m_L/m_C will be of order 1/4 to 1/2 (Fig. 6), and thus (albeit the surface may be renewed by magmatism) D_L/d_B will be close to 1.

CONCLUSIONS

1. A difference in approach versus previous ejecta accumulation studies is that here the model is keyed to assumptions for the largest impact crater size (D_L), with no explicit modeling of time. In conjunction with assumed cratering size-distribution exponent b (constrained by comparison with present-day asteroids), D_L implicitly constrains the approximate sizes of all other craters large enough to be significant contributors to the final megaregolith. Another noteworthy difference is that the typical D_L is constrained (albeit still only loosely) using a more sophisticated model (Bottke et al. 2005a, 2005b) for estimating the impactor mass m_C that, at a given velocity, results in catastrophic disruption.
2. Globally averaged ejecta accumulation thickness z_A is relatively constant over a wide range of body diameter d_B for any given largest impactor mass ratio m_L/m_B of order 0.001 (along with constant b and impact velocity v_i). In general, for $b = 2$ and $v_i = 5$ km s^{-1} the relationship is z_A (in km) $\sim 300(m_L/m_B)^{0.8}$. As a specific example, $m_L/m_B = 0.001$ results in z_A ranging from 1.0 to 1.3 km for all d_B between 50 and 800 km.
3. For planetesimals, the largest impactor mass m_L is more likely some consistently major fraction of the catastrophic-disruption mass m_C. The total ejecta accumulation z_A (assuming $b \sim 2$ and $v_i = 5$ km s^{-1}) is then roughly proportional to d_B, with $z_A/d_B \sim 0.04(m_L/m_C)$; i.e., assuming m_L/m_C is between 1/10 and 2/3, z_A will be 1–5% of the body's radius r_B.
4. However, ejecta accumulations on bodies with $d_B \sim 100$ km may be significantly (roughly a factor of 1.6) higher than implied by the nominal model. This diameter is the "sweet spot" for high m_C/m_B (and thus D_L/d_B). A 1000 km body, for example, is implied to have lower D_L/d_B by (on average) a factor of approximately 0.86. The main advantage is from simple proportionality to $(D_L/d_B)^3$ (Equation 2*b*), but craters with very high D_L/d_B ($> \sim 1$) also excavate to significantly deeper (lower r/r_B) levels, so they enhance the yield of fresh, as opposed to recycled, ejecta.
5. Global ejecta accumulations estimated by this approach are higher than in the classic Housen et al.'s (1979) study by a factor of roughly 10. This revision is caused mainly by higher (typical) m_L that are suggested by higher estimated m_C.
6. For $b \sim 2$, the single largest crater will generally contribute close to 50% of the total of new (nonrecycled) ejecta. Considering the stochastic nature of the cratering process, there are probably many cases where the single largest crater contributes $>> 50\%$.
7. For modeling of the thermal effects of ejecta accumulation among different bodies, significant stochastic variations probably arise from two effects: concentration of ejecta mass into a relative few large fragments (although if formed relatively early these may be largely eroded down by later cratering); and stochastically uneven ejecta distribution, especially on relatively small bodies.
8. In cases of stochastically uneven ejecta distribution, the lower k associated with a thin layer of regolith (sensu stricto; i.e., uncommonly fine-grained and porous ejecta-debris produced by thorough small-scale, high-b gardening of the surface) probably to some extent compensates for low regional accumulation thicknesses. Otherwise, however, regoliths thick enough to have major thermal consequences probably seldom develop, because regolith tends to be destroyed by churning-dilution during the landings of much greater volumes of ejecta from the biggest handful of craters.
9. For any given radial position r/r_B, the pressure sensitivity of the sintering process makes it effective at far lower temperature T_S on larger ($d_B >> 100$ km) bodies.
10. Planetesimals ~ 100 km in diameter may be surprisingly well suited (comparable to bodies 2–3 times larges in d_B, assuming equal heat production) for attaining temperatures associated with widespread melting, for four reasons: (1) the approximately 100 km "sweet spot" for high D_L/d_B; (2) the value of b for impactors that have near-critical mass (m_i/m_C of order 1/3 to 1) declines markedly as d_B increases from $\sim$ 80 to $\sim$220 km; (3) generally higher T_S; and (4) on such relatively small planetesimals, the thickness z_{skin} of the thermally graded layer during rapid whole-body heating is likely to exceed z_A, whereas in large bodies z_{skin} may sometimes be less than z_A.
11. A water-rich composition may be a significant disadvantage in terms of planetesimal heating. The

shallow interior may be densified by aqueous metamorphism. Also, if the deep megaregolith is water-rich it will have a lower T_S.

12. Development of a megaregolith thick and porous enough to have important thermal evolution consequences is practically inevitable. However, the cratering process that generates megaregolith is stochastic enough to leave great scope for diversity of outcome.
13. More work is needed, especially on two issues: heat loss with a thick but uneven coverage of megaregolith, and pressure-aided anhydrous sintering.

Acknowledgments—I thank Dan Durda and Lionel Wilson for helpful, constructive reviews; also Jeroen Molemaker and John Wasson for helpful advice. This work was supported by NASA grant NNX09AE31G.

Editorial Handling—Dr. Michael Gaffey

REFERENCES

Akechi K. and Hara Z. 1979. Sintering of loosely packed metal powder. In *Sintering: New developments*, edited by Ristic M. M. New York: Elsevier. pp. 67–75.

Akridge G., Benoit P. H., and Sears D. W. G. 1998. Regolith and megaregolith formation of H-chondrites: Thermal constraints on the parent body. *Icarus* 132:185–195.

Alister M., Brula G., Lecomte F., Reymond J. P., and Vergnon P. 1979. Influence of the structure, pressing, atmosphere and doping on the sintering of spherical particles of titanium dioxide. In *Sintering: New developments*, edited by Ristic M. M. New York: Elsevier. pp. 150–159.

Anderson J. L. B., Schultz P. H., and Heineck J. T. 2003. A test of Maxwell's Z model using inverse modeling (abstract #1762). 34th Lunar and Planetary Science Conference. CD-ROM.

Asphaug E. 1997. Impact origin of the Vesta family. *Meteoritics & Planetary Science* 32:965–980.

Asphaug E. 2008. Critical crater diameter and asteroid impact seismology. *Meteoritics & Planetary Science* 43: 1075–1084.

Asphaug E. 2009. Growth and evolution of asteroids. *Annual Review of Earth and Planetary Sciences* 37:413–448.

Barnett W. 2004. Subsidence breccias in kimberlite pipes—An application of fractal analysis. *Lithos* 76:299–316.

Benz W. and Jutzi M. 2007. Collision and impact simulations including porosity. In *Near earth objects, our celestial neighbors: Opportunity and risk*. Proceedings, I.A.U. Symposium No. 236, edited by Milani A., Valsecchi G. B., and Vokrouhlicky D. Cambridge, UK: Cambridge University Press. pp. 223–232.

Blenkinsop T. G. 1991. Cataclasis and processes of particle size reduction. *Pure and Applied Geophysics* 136:59–86.

Bottke W. F. Jr., Durda D. D., Nesvorný D., Jedicke R., Morbidelli A., Vokrouhlický D., and Levison H. 2005a. The fossilized size distribution of the main asteroid belt. *Icarus* 175:111–140.

Bottke W. F. Jr., Durda D. D., Nesvorný D., Jedicke R., Morbidelli A., Vokrouhlicky D., and Levison H. F. 2005b. Linking the collisional history of the main asteroid belt to its dynamical excitation and depletion. *Icarus* 179:63–94.

Brearley A. J. 2006. The action of water. In *Meteorites and the early solar system II*, edited by Lauretta D. S. and McSween H. Y. Jr. Tucson, AZ: The University of Arizona Press. pp. 584–624.

Britt D. T., Yeomans D., Housen K., and Consolmagno G. 2002. Asteroid density, porosity, and structure. In *Asteroids III*, edited by Bottke W. F., Cellino A., Paolicchi P., and Binzel R. P. Tucson, AZ: The University of Arizona Press. pp. 485–500.

Carrier W. D. III, Olhoeft G. R., and Mendell W. 1991. Physical properties of the lunar surface. In *Lunar sourcebook, A user's guide to the Moon*, edited by Heiken G. H., Vaniman D. T., and French B. M. Cambridge, UK: Cambridge University Press. pp. 475–594.

Carslaw H. S. and Jaeger J. C. 1959. *Conduction of heat in solids*. New York: Oxford University Press. 510 p.

Chapman C. R., Merline W. J., Thomas P. C., Joseph J., Cheng A. F., and Izenberg N. 2002. Impact history of Eros: Craters and boulders. *Icarus* 155:104–118.

Ciesla F. J., Collins G. S., and Davison T. M. 2009. The thermal evolution of post-impact planetesimals (abstract #1086). 40th Lunar and Planetary Science Conference. CD-ROM.

Cintala M. J. and McBride K. M. 1995. Block distributions on the lunar surface: A comparison between measurements obtained from surface and orbital photography. NASA Johnson Space Center Technical Memorandum 104804, 46 pp.

Cintala M. J., Head J. W., and Veverka J. 1978. Characteristics of the cratering process on small satellites and asteroids. Proceedings, 9th Lunar and Planetary Science Conference. pp. 3803–3831.

Cintala M. J., Head J. W., and Wilson L. 1979. The nature and effects of impact cratering on small bodies. In *Asteroids*, edited by Gehrels T. Tucson, AZ: The University of Arizona Press. pp. 579–600.

Cooper R. F. and Kohlstedt D. L. 1982. Interfacial energies in the olivine-basalt system. *Geophysics* 12:217–228.

Croft S. K. 1980. Cratering flow fields: Implications for the excavation and transient expansion stages of crater formation. Proceedings, 11th Lunar and Planetary Science Conference. pp. 2347–2378.

Cukierman M., Klein L., Scherer G., Hopper R. W., and Uhlmann D. R. 1973. Viscous flow and crystallization behavior of selected lunar compositions. Proceedings, 4th Lunar Science Conference. pp. 2685–2696.

Dohnanyi J. S. 1969. Collisional models of asteroids and their debris. *Journal of Geophysical Research* 74:2531–2554.

Faul U. H. and Jackson I. 2007. Diffusion creep of dry, melt-free olivine. *Journal of Geophysical Research* 112:B04204.

Geissler P., Petit J.-M., Durda D. D., Greenberg R., Bottke W., and Nolan M. 1996. Erosion and ejecta reaccretion on 243 Ida and its Moon. *Icarus* 120:140–157.

German R. M. 1996. *Sintering theory and practice*. New York: Wiley. 550 pp.

Ghosh A. and McSween H. Y. Jr. 1998. A thermal model for the differentiation of asteroid 4 Vesta, based on radiogenic heating. *Icarus* 134:187–206.

Golombek M. P. 1979. Structural analysis of lunar grabens and the shallow crustal structure of the Moon. *Journal of Geophysical Research* 84:4657–4666.

Grimm R. E. and McSween H. Y. Jr. 1989. Water and the thermal evolution of carbonaceous chondrite parent bodies. *Icarus* 82:244–280.

Hammond N. P., Nimmo F., and Korycansky D. 2009. Hydrocode modeling of the South Pole Aitken basin-forming impact (abstract #1455). 40th Lunar and Planetary Science Conference. CD-ROM.

Hartmann W. K. 1973. Ancient lunar mega-regolith and subsurface structure. *Icarus* 18:634–636.

Haskin L. A., Moss W. E., and McKinnon W. B. 2003. On estimating the contributions of basin ejecta to regolith deposits at lunar sites. *Meteoritics & Planetary Science* 38:13–33.

Head J. W. 1976. The significance of substrate characteristics in determining morphology and morphometry of lunar craters. Proceedings, 7th Lunar Science Conference. pp. 2913–2929.

Hevey P. and Sanders I. S. 2006. A model for planetesimal meltdown by ^{26}Al and its implications for meteorite parent bodies. *Meteoritics & Planetary Science* 41:95–106.

Hofmeister A. M. 1999. Mantle values of thermal conductivity and the geotherm from photon lifetimes. *Science* 283:1699–1706.

Hofmeister A. M. 2005. Dependence of diffusive radiative transfer on grain-size, temperature, and Fe-content: Implications for mantle processes. *Journal of Geodynamics* 40:51–72.

Holsapple K. A. 1993. The scaling of impact processes in planetary sciences. *Annual Review of Earth and Planetary Sciences* 21:333–373.

Holsapple K. A. 2003. *Theory and equations for "Craters from Impacts and Explosions."* St. Louis, MO: Washington University. 9 p. http://keith.aa.washington.edu/craterdata/scaling/index.htm. Accessed November 20, 2010.

Horai K. and Winkler J. L. 1976. Thermal diffusivity of four Apollo 17 rock samples. Proceedings, 7th Lunar Science Conference. pp. 3183–3204.

Horai K. and Winkler J. L. Jr. 1980. Thermal diffusivity of two Apollo 11 samples, 10020,44 and 10065,23: Effect of petrofabrics on the thermal conductivity of porous lunar rocks under vacuum. Proceedings, 11th Lunar and Planetary Science Conference. pp. 1777–1788.

Housen K. R. and Holsapple K. A. 2003. Impact cratering on porous asteroids. *Icarus* 163:102–119.

Housen K. R. and Wilkening L. L. 1982. Regoliths on small bodies in the solar system. *Annual Review of Earth and Planetary Sciences* 10:355–376.

Housen K. R., Wilkening L. L., Chapman C. R., and Greenberg R. J. 1979. Asteroidal regoliths. *Icarus* 39:317–352.

Housen K. R., Schmidt R. M., and Holsapple K. A. 1983. Crater ejecta scaling laws: Fundamental forms based on dimensional analysis. *Journal of Geophysical Research* 88:2485–2499.

Housen K. R., Holsapple K. A., and Voss M. E. 1999. Compaction as the origin of the unusual craters on asteroid Mathilde. *Nature* 402:155–157.

Kang S.-J. L. 2005. *Sintering: Densification, grain growth & microstructure*. Amsterdam: Elsevier. 265 p.

Karato S.-I., Paterson M. S., and FitzGerald J. D. 1986. Rheology of synthetic olivine aggregates: Influence of grain size and water. *Journal of Geophysical Research* 91:8151–8176.

Kelley M. S., Vilas F., Gaffey M. J., and Abell P. A. 2003. Quantified mineralogical evidence for a common origin of 1929 Kollaa with 4 Vesta and the HED meteorites. *Icarus* 165:215–218.

Langseth M. G., Keihm S. J., and Peters K. 1976. Revised lunar heat-flow values. Proceedings, 7th Lunar Science Conference. pp. 3143–3171.

Lee P., Veverka J., Thomas P. C., Helfenstein P., Belton M. J. S., Chapman C. R., Greeley R., Pappalardo R. T., Sullivan R., and Head J. W. III. 1996. Ejecta blocks on 243 Ida and on other asteroids. *Icarus* 120:87–105.

Leliwa-Kopystyński J., Burchell M. J., and Lowen D. 2008. Impact cratering and the break up of small bodies of the solar system. *Icarus* 195:817–826.

Maxwell D. 1977. Simple Z modeling of cratering, ejection, and the overturned flap. In *Impact and explosion cratering*, edited by Roddy J., Pepin R. O., and Merrill R. B. New York: Pergamon. pp. 1003–1008.

McSween H. Y. Jr. and Labotka T. C. 1993. Oxidation during metamorphism of the ordinary chondrites. *Geochimica et Cosmochimica Acta* 57:1105–1114.

Melosh H. J. 1989. *Impact cratering: A geologic process*. New York: Oxford University Press. 245 p.

Merk R., Breuer D., and Spohn T. 2002. Numerical modeling of ^{26}Al-induced radioactive melting of asteroids considering accretion. *Icarus* 159:183–191.

Nolan M. C., Asphaug E., Greenberg R., and Melosh H. J. 2001. Impacts on asteroids: Fragmentation, regolith transport, and disruption. *Icarus* 153:1–15.

Nyquist L. E., Kleine T., Shih C.-Y., and Reese Y. D. 2009. The distribution of short-lived radioisotopes in the early solar system and the chronology of asteroid accretion, differentiation, and secondary mineralization. *Geochimica et Cosmochimica Acta* 73:5115–5136.

Oberbeck V. R. 1975. The role of ballistic sedimentation in lunar stratigraphy. *Reviews of Geophysics and Space Physics* 13:337–362.

O'Brien D. P. and Greenberg R. 2005. The collisional and dynamical evolution of the main-belt and NEA size distributions. *Icarus* 178:179–212.

Petro N. E. and Pieters C. M. 2008. The lunar-wide effects of basin ejecta distribution on the early megaregolith. *Meteoritics & Planetary Science* 43:1517–1529.

Poppe T. 2003. Sintering of highly porous silica-particle samples: Analogues of early solar-system aggregates. *Icarus* 164:139–148.

Richardson J. E. 2009. Cratering saturation and equilibrium: A new model looks at an old problem. *Icarus* 204:697–715.

Richardson J. E. Jr., Melosh H. J., Greenberg R. J., and O'Brien D. P. 2005. The global effects of impact-induced seismic activity on fractured asteroid surface morphology. *Icarus* 179:325–349.

Robinson M. S., Thomas P. C., Veverka J., Murchie S. L., and Wilcox B. B. 2002. The geology of 433 Eros. *Meteoritics & Planetary Science* 37:1651–1684.

Russell C. T., Coradini A., Christensen U., De Sanctis M. C., Feldman W. C., Jaumann R., Keller H. U., Konopliv A. S., McCord T. B., McFadden L. A., McSween H. Y., Mottola S., Neukum G., Pieters C. M., Prettyman T. H., Raymond C. A., Smith D. E., Sykes M. V., Williams B. G., Wise J., and Zuber M. T. 2004. Dawn: A journey in space and time. *Planetary and Space Science* 52:465–489.

Sahijpal S., Soni P., and Gupta G. 2007. Numerical simulations of the differentiation of accreting planetesimals with ^{26}Al and ^{60}Fe as the heat sources. *Meteoritics & Planetary Science* 42:1529–1548.

Schatz F. J. and Simmons G. 1972. Thermal conductivity of earth materials at high temperatures. *Journal of Geophysical Research* 72:6966–6983.
Schwenn M. B. and Goetze C. 1978. Creep of olivine during hot-pressing. *Tectonophysics* 48:41–60.
Scott E. R. D. and Wilson L. 2005. Meteoritic and other constraints on the internal structure and impact history of small asteroids. *Icarus* 174:46–53.
Shankland T. J., Nitsan U., and Duba A. G. 1979. Optical absorption and radiative heat transport in olivine at high temperature. *Journal of Geophysical Research* 84:1603–1610.
Shoemaker E. M., Hait M. H., Swann G. A., Schleicher D. L., Schaber G. G., Sutton R. L., Dahlem D. H., Goddard E. N., and Waters A. C. 1969. Origin of the lunar regolith at Tranquillity Base. Proceedings, Apollo 11 Lunar Science Conference. pp. 2399–2412.
Simonds C. H. 1973. Sintering and hot pressing of Fra Mauro composition glass and the lithification of lunar breccias. *American Journal of Science* 273:428–439.
Stesky R. M. 1978. Experimental compressional wave velocity measurements in compacting powders under high vacuum: Applications to lunar crustal sounding. Proceedings, 9th Lunar and Planetary Science Conference. pp. 3637–3649.
Sucec J. 1975. *Heat transfer*. New York: Simon and Schuster. 604 p.
Sullivan R. J., Thomas P. C., Murchie S. L., and Robinson M. S. 2002. Asteroid geology from Galileo and NEAR Shoemaker data. In *Asteroids III*, edited by Bottke W. F., Cellino A., Paolicchi P., and Binzel R. P. Tucson, AZ: The University of Arizona Press. pp. 331–350.
Thomas P. C., Binzel R. P., Gaffey M. J., Storrs A. D., Wells E. N., and Zellner B. H. 1997. Impact excavation on Asteroid 4 Vesta: Hubble Space Telescope results. *Science* 277:1492–1495.
Thompson T. W., Roberts W. J., Hartmann W. K., Shorthill R. W., and Zisk S. H. 1979. Blocky craters: Implications about the lunar megaregolith. *The Moon and the Planets* 21:319–342.
Thompson T. W., Campbell B. A., Ghent R. R., and Hawke B. R. 2009. Rugged crater ejecta as a guide to megaregolith thickness in the southern nearside of the Moon. *Geology* 37:655–658.
Turcotte D. L. and Schubert G. 1982. *Geodynamics: Applications of continuum physics to geological problems*. New York: Wiley. 450 p.
Wada K., Senshu H., and Matsui T. 2004. A plausibility of Z-model (abstract #1520). 35th Lunar and Planetary Science Conference. CD-ROM.
Ward S. N. 2002. Planetary cratering: A probabilistic approach. *Journal of Geophysical Research—Planets* 107:E001343.
Warren P. H. 2001a. Porosities of lunar meteorites: Strength, porosity, and petrologic screening during the meteorite delivery process. *Journal of Geophysical Research—Planets* 106:10101–10112.
Warren P. H. 2001b. Compositional structure within the lunar crust as constrained by Lunar Prospector thorium data. *Geophysical Research Letters* 28:2565–2568.
Warren P. H. and Huber H. 2006. Ureilite petrogenesis: A limited role for smelting during anatexis and catastrophic disruption. *Meteoritics & Planetary Science* 41:835–849.
Warren P. H. and Rasmussen K. L. 1987. Megaregolith insulation, internal temperatures, and bulk uranium content of the Moon. *Journal of Geophysical Research* 92:3453–3465.
Wechsler A. E., Glasser P. E., and Fountain J. A. 1972. Thermal properties of granular materials. In *Thermal characteristics of the Moon*, edited by Lucas J. W. Cambridge, Massachusetts: MIT Press. pp. 215–241.
Weidenschilling S. J. and Cuzzi J. N. 2006. Accretion dynamics and time scales: Relation to chondrites. In *Meteorites and the early solar system II*, edited by Lauretta D. S. and McSween H. Y. Tucson, AZ: The University of Arizona Press. pp. 473–485.
Wilhelms D. E. 1987. *The geologic history of the Moon*. USGS Professional Paper 1348. Washington, D.C.: U.S. Geological Survey. 302 p.
Wilson L., Keil K., and Love S. J. 1999. The internal structures and densities of asteroids. *Meteoritics & Planetary Science* 34:479–483.
Wilson L., Goodrich C. A., and Van Orman J. A. 2008. Thermal evolution and physics of melt extraction on the ureilite parent body. *Geochimica et Cosmochimica Acta* 72:6154–6176.
Yamamoto S., Barnouin-Jha O. S., Toriumi T., Sugita S., and Matsui T. 2009. An empirical model for transient crater growth in granular targets based on direct observations. *Icarus* 203:310–319.
Yomogida K. and Matsui T. 1984. Multiple parent bodies of ordinary chondrites. *Earth and Planetary Science Letters* 68:34–42.
Young E. D., Zhang K. K., and Schubert G. 2003. Conditions for pore water convection within carbonaceous chondrite parent bodies—Implications for planetesimal size and heat production. *Earth and Planetary Science Letters* 213:249–259.
Zagar L. 1979. Theoretical aspects of sintering glass powders. In *Sintering: New developments*, edited by Ristic M. New York: Elsevier. pp. 57–64.
Zolensky M. E. 1995. Cyclical regolith processes on hydrous asteroids (abstract). *Meteoritics & Planetary Science* 30:A606–A607.

SUPPORTING INFORMATION

Additional supporting information may be found in the online version of this article:

Fig. S1. This is identical to Fig. 20, except here the axes have been reformatted to log-log scaling, which results in near-linear curves for each set of (fixed diffusivity and θ) results. However, decay of the heat source (^{26}Al) causes the curves to deviate from parallel-linearity toward the low-t end of the diagram. Curves are shown for seven different possible values of θ, i.e., $(T_{base} - T_{surface})/(T_{deep} - T_{surface})$; and for three different values of thermal diffusivity κ. To a fair approximation, $\kappa \sim 10^{-6}$ (m^2 s^{-1}) corresponds to a skin that consists of solid rock, 10^{-7} corresponds to a skin of porous-rocky megaregolith, and 10^{-8} to a skin of powdery regolith (sensu stricto).

Fig. S2. This is analogous to Fig. 20, except here post-t_0 heating (by ^{26}Al) is ignored, and consequently the z_{skin} results are slightly greater. Curves are shown

for seven different possible values of θ, i.e., $(T_{base} - T_{surface})/(T_{deep} - T_{surface})$; and for three different values of thermal diffusivity κ. To a fair approximation, $\kappa \sim 10^{-6}$ (m^2 s^{-1}) corresponds to a skin that consists of solid rock, 10^{-7} corresponds to a skin of porous-rocky megaregolith, and 10^{-8} to a skin of powdery regolith (sensu stricto).

Fig. S3. This is identical to Fig. S2, except here the axes have been reformatted to log-log scaling, which results in linear curves for each set of (fixed diffusivity and θ) results. Curves are shown for seven different possible values of θ, i.e., $(T_{base} - T_{surface})/(T_{deep} - T_{surface})$; and for three different values of thermal diffusivity κ. To a fair approximation, $\kappa \sim 10^{-6}$ (m^2 s^{-1}) corresponds to a skin that consists of solid rock, 10^{-7} corresponds to a skin of porous-rocky megaregolith, and 10^{-8} to a skin of powdery regolith (sensu stricto).